



# Damage detection of civil structures based on hybrid optimization algorithm and combined correlation function of heterogeneous responses

Guangcai Zhang<sup>a</sup>, Chunfeng Wan<sup>a,\*</sup>, Zhiyuan Yang<sup>a</sup>, Liyu Xie<sup>b</sup>, Songtao Xue<sup>b,c,\*\*</sup>

<sup>a</sup> Key Laboratory of concrete and prestressed concrete structure of Ministry of Education, Southeast University, Nanjing, China

<sup>b</sup> Department of Disaster Mitigation for Structures, Tongji University, Shanghai 200092, China

<sup>c</sup> Department of Architecture, Tohoku Institute of Technology, Sendai, Japan

## ARTICLE INFO

### Keywords:

Broyden-Fletcher-Goldfarb-Shanno  
Combined correlation function  
Damage detection  
Heterogeneous responses  
Hybrid optimization algorithm  
Output-only method

## ABSTRACT

Accurate and robust damage detection of civil structures subjected to ambient excitations is crucial for ensuring safety and maintaining structural integrity. Heuristic algorithms and traditional reference point-defined correlation function methods have been employed in recent years. However, most single-method optimization strategies suffer from drawbacks such as slow convergence for global search optimizers and strong reliance on the initial guess for local search optimizers. Additionally, selecting the optimal reference point a priori is difficult, and identification accuracy would be severely compromised if the selected reference point exhibits poor response sensitivity to damage. To overcome these limitations, this paper proposes a novel output-only damage detection method for civil structures based on the hybrid optimization algorithm and combined correlation function of heterogeneous responses. The hybrid optimization algorithm integrates the local search operator of the Broyden-Fletcher-Goldfarb-Shanno (BFGS) algorithm into the global search optimizer of the hybrid Jaya and differential evolution algorithm (HJDEA), leveraging their comprehensive exploration and good convergence capacities. A new objective function is formulated based on the combined correlation function among acceleration and strain, eliminating the need for a reference point. To demonstrate the effectiveness of the proposed method, numerical studies on the Guangzhou new TV tower and a complex three-dimensional space truss structure are conducted. Furthermore, the effect of noise level, sampling frequency, sampling duration, and number of data points are investigated. The results show that the proposed method based on HJDEA-BFGS algorithm and combined correlation function with heterogeneous responses can achieve less than 0.4% mean error for varying damage scenarios and maintains robustness under noise levels up to 20%, demonstrating its reliability for real-world applications.

## 1. Introduction

During the long-term service life, continuous health monitoring and damage assessment on the existing civil structures are remarkably important to evaluate health status and predict the failure of the structures [1]. Over the past few decades, there has been a significant increase in attention towards structural damage identification, such as digital image correlation [2], vision-based method [3], particularly focusing on vibration-based damage identification approaches [4–7]. The core principle of these methods is that structural damage would result in changes to its physical properties, such as mass, damping, and

stiffness. These changes lead to detectable variations in the structure's dynamic characteristics. By analyzing these dynamic responses, it is feasible to inversely evaluate structural damages.

The vibration-based damage identification approaches can be broadly categorized into two types: frequency domain methods and time domain methods. In frequency domain methods, the structural health state is assessed by minimizing the discrepancies in damage-sensitive features between the real structure and its finite element model (FEM). However, lower order modes are often insensitive to small damages, while higher order modes are challenging to accurately capture from the real structure due to limitations in external excitation and

\* Corresponding author.

\*\* Corresponding author at: Department of Disaster Mitigation for Structures, Tongji University, Shanghai 200092, China.

E-mail addresses: [guangcaizhang@seu.edu.cn](mailto:guangcaizhang@seu.edu.cn) (G. Zhang), [wan@seu.edu.cn](mailto:wan@seu.edu.cn) (C. Wan), [zhiyuanyang2021@yahoo.com](mailto:zhiyuanyang2021@yahoo.com) (Z. Yang), [liyuxie@tongji.edu.cn](mailto:liyuxie@tongji.edu.cn) (L. Xie), [xue@tongji.edu.cn](mailto:xue@tongji.edu.cn) (S. Xue).

<https://doi.org/10.1016/j.measurement.2025.116678>

Received 3 July 2024; Received in revised form 6 December 2024; Accepted 4 January 2025

Available online 6 January 2025

0263-2241/© 2025 Elsevier Ltd. All rights reserved, including those for text and data mining, AI training, and similar technologies.

the adverse effects of environmental variations and measurement noise. These challenges limit the applicability of frequency domain methods [8]. Instead, time domain methods generally identify structural damages directly using measured structural vibration signals. Some classical time domain methods, such as the iterative least square method [9], the dynamic response sensitivity-based method [10], the extend Kalman filter method [11], the particle filter method [12], have been proposed and validated to be successful in structural damage identification. Basically, these classical methods have solid background of mathematical theories, while a good initial guess of the unknown parameters and proper function gradient are required. Furthermore, inherent point-to-point search mechanism makes these methods easier to fall into the local optimum.

In contrast, computational intelligence approaches [13], e.g., machine learning methods [14], especially for heuristic algorithms [15,16], can not only avoid the abovementioned limitations, but also nicely solve complicated optimization problems with multi-modality, nonlinearity, discontinuity. In recent years, various non-classical methods, parallel genetic algorithms (GA) [17], tree seeds algorithm [18], grey wolf optimization algorithm [19], improved grasshopper optimization algorithm [20], improved reptile search algorithm [21], etc., have been proposed and adopted due to their advantages of simplicity, flexibility and robustness. Therefore, it can be found from these researches that heuristic algorithms show promising performance in structural damage identification, while they still face some challenges, such as

(a) For heuristic algorithms, trial-and-error procedures are typically implemented to tune appropriate algorithm-specific parameters before tackling various optimization problems. This approach inevitably wastes significant computational resources. Additionally, considerable evaluations of the objective function are still required even after the neighborhood of the best solution is approached.

(b) Some recent progress has been made in the inverse problem of force reconstruction, such as regularization approaches [22–24], but structural damage and unknown loads may exist simultaneously. The unavailability of external excitation acting on civil structures, such as wind load, traffic load, or wave load, makes structural damage identification challenging. Developing more output-only methods to identify structural damages under ambient excitations using heterogeneous responses, including strains and accelerations, is appealing because it aligns more closely with the actual operational state of infrastructure.

To address the first challenge, several efforts have been made. Rao introduced a novel population-based stochastic optimization algorithm, named Jaya algorithm, to tackle complex optimization problems [25]. The fundamental principle of Jaya algorithm is that offspring move towards success by approaching the best solution and avoid failure by moving away from the worst solution. The key advantage of Jaya algorithm is that it does not require any algorithm-specific parameters, which significantly enhances its applicability, efficiency, and robustness [26]. However, as an emerging swarm intelligence algorithm, Jaya algorithm may exhibit an unfavorable convergence rate due to a heavy reliance on local search and tend to fall into local optima because of excessive neglect of global search [27]. To improve Jaya algorithm, Belhadj et al. [28] proposed an enhanced version by introducing three modifications into the original Jaya scheme. Ding et al. [29] integrated k-means clustering, Hooke–Jeeves pattern search, and a linear population reduction strategy into Jaya algorithm. They concluded that incorporating a suitable local search operator to update the best-so-far solution is one of the most effective and efficient approaches, which was also employed in some previous studies [30,31]. The Nelder–Mead simplex method was utilized as a local search operator to improve the performance of artificial bee colony algorithm [32]. The Broyden–Fletcher–Goldfarb–Shanno (BFGS) algorithm [33] is a gradient-based quasi-Newton method that guides the best-so-far solution to promising regions of the search space. Therefore, in this study, we propose a new hybrid optimization algorithm, the hybrid Jaya and differential evolution algorithm-BFGS (HJDEA-BFGS), by integrating the local search

operator of BFGS into the global search optimizer of the HJDEA algorithm to improve convergence speed and identification accuracy. The global search optimizer HJDEA includes a mutation pool composed of Jaya mutation and DE/rand/2 strategies, along with two key modifications. The first modification involves generating a more uniform initial population using the Hammersley sequence rather than a random manner. The second modification refines the best solution through Lévy flight search to help escape local optima. The HJDEA provides a good initial point quickly refined by the BFGS algorithm.

To address the second challenge, some output-only damage identification methods under unknown stationary ambient excitations have been developed and applied [34–36]. An auto/cross-correlation function of acceleration response-based identification method was proposed to identify damages in a laboratory four-story steel frame model [37]. Correlation functions were extended to damage identification of the ASCE benchmark frame structure using four different evolutionary algorithms [38]. Acceleration responses can effectively monitor the health state at a global level, but the nature of structural damage is predominantly a local phenomenon. Consequently, low levels of damage may not be sufficiently reflected in global acceleration responses. In contrast, strain responses are more sensitive to minor damages than acceleration measurements, as strain gauges can capture detailed local information about small or minor damages more effectively. To this end, Zhang et al. [39] presented correlation functions of strain responses and proved their effectiveness in damage detection of the steel grid benchmark structure. Li et al. [40] utilized cross-correlation function amplitude vector of the dynamic strain for structural damage detection. Although strain responses have shown promising performance in detecting damages, considerable strain gauges are normally required. This requirement limits the practical application of strain response-based methods, as they can only collect point-to-point local information near the sensors.

Some damage identification methods based on data fusion have been attempted, considering the complementary characteristics of heterogeneous responses. For example, strain and acceleration responses have been applied to estimate parameters of foundation systems [41] and detect bolt loosening in steel frames [42]. Considering the merits of correlation function-based damage identification methods and data fusion, the correlation function among hybrid acceleration and strain responses was proposed [43]. It is noted that a reference point for correlation functions is necessarily required in the aforementioned methods. Reference point plays a vital role in the accuracy and reliability of damage identification results. If the selected reference point exhibits poor sensitivity to damage, the identification accuracy can be severely compromised [44]. Moreover, determining the optimal reference point a priori in real-world applications is difficult, especially for large-scale and complex structures, since multiple potential damages may exist and the variability in response sensitivity across the structure is high. To address these challenges, a reference point-free method based on the combined correlation function of heterogeneous responses is proposed, which can avoid misidentification of damage caused by inappropriate selection of the reference point.

The basic idea of this paper is to develop an output-only damage detection method for civil structures subjected to unknown ambient excitations based on the hybrid optimization algorithm and the combined correlation function of heterogeneous responses. To enhance convergence speed and optimization performance, an efficient HJDEA-BFGS algorithm is proposed by integrating the local search operator of BFGS into the global search optimizer of HJDEA. This integration achieves a balanced approach between exploration (global search capability) and exploitation (local search capability). The high convergence rate and accuracy are attained with the assistance of BFGS, using the identified solution from HJDEA as the initial point. Additionally, a combined correlation function is introduced to formulate the objective function, eliminating the requirement for the reference point. The optimization capability of the proposed HJDEA-BFGS is validated using mathematical benchmark functions. Numerical studies on the

Guangzhou New TV tower and a 39-bar three-dimensional space truss structure under ambient excitations are conducted. Identified results show that unlike prior methods reliant on predefined reference points or idealized conditions, the proposed method achieves a noise tolerance of 20 % and identification accuracy of less than 0.4 % mean error in the numerical studies on the Guangzhou new TV tower and a complex three-dimensional space truss structure, as validated against GA, GBABC, Jaya, HJDEA.

## 2. Identification algorithms

### 2.1. Hybrid Jaya and differential evolution algorithm

In this section, the hybrid Jaya and differential evolution algorithm (HJDEA) is proposed and elaborated. Mutation pool composed of Jaya and DE, and then two key modifications are introduced.

#### 2.1.1. Mutation pool based on Jaya and DE

Jaya algorithm comprises four main steps: initialization, individual updating, greedy selection, and result output.

Initially, individuals are randomly generated in the predefined upper and lower search limits

$$X_{i,j} = L_{i,j} + \text{rand}(0, 1) \times (U_{i,j} - L_{i,j}), \quad i = 1, 2, \dots, NP; \quad j = 1, 2, \dots, Dim \quad (1)$$

where  $X_{i,j}$  means the  $j$ -th variables of the  $i$ -th candidate solution;  $\text{rand}(0, 1)$  stands for the random number taken from the range of  $[0, 1]$ ;  $U_{i,j}$  and  $L_{i,j}$  are the upper and lower search space limits;  $NP$  and  $Dim$  represent the population size and the number of unknown parameters, respectively.

The core idea of Jaya algorithm is that offsprings would move towards the best solution meanwhile avoid the worst solution. The offspring  $X'_{i,j,G}$  can be updated as follows

$$X'_{i,j,G} = X_{i,j,G} + \text{rand}_1 \times (X_{\text{best},j,G} - |X_{i,j,G}|) - \text{rand}_2 \times (X_{\text{worst},j,G} - |X_{i,j,G}|) \quad (2)$$

where  $X_{i,j,G}$  represents the  $j$ -th variable of the  $i$ -th individual at the  $G$ -iteration;  $\text{rand}_1$  and  $\text{rand}_2$  stand for two random numbers within the range of  $[0, 1]$ ;  $X_{\text{best},j,G}$  and  $X_{\text{worst},j,G}$  mean the values of the  $j$ -th variable of the best and worst solution, respectively.

Then, greedy selection mechanism is implemented to select better solution using

$$X_{i,G+1} = \begin{cases} X'_{i,G} & \text{Obj}(X'_{i,G}) \leq \text{Obj}(X_{i,G}) \\ X_{i,G} & \text{otherwise} \end{cases} \quad (3)$$

where  $X_{i,G}$  and  $X'_{i,G}$  are the  $i$ -th individual at the  $G$ -iteration and its updated value;  $\text{Obj}$  represents the value of objective function. It can be found from Eq. (3) that the solution with better objective function value will survive to next generation. Finally, the best solution and optimal value are output.

It is noted that Jaya algorithm update individuals with  $X_{\text{best}}$  and  $X_{\text{worst}}$ . Although it can speed up the convergence rate and improve the local search capability, the population diversity and global search capability may decrease with the iterations. To this end, DE/rand/2 mutation operation of DE algorithm is introduced as

$$V_{i,G+1} = X_{r1,G} + \text{rand}_1 \times (X_{r2,G} - X_{r3,G}) + \text{rand}_2 \times (X_{r4,G} - X_{r5,G}) \quad (4)$$

where  $V_{i,G+1}$  stands for the mutated individual;  $X_{r1,G}$ ,  $X_{r2,G}$ ,  $X_{r3,G}$ ,  $X_{r4,G}$  and  $X_{r5,G}$  are randomly selected individuals from the population,  $r1 \neq r2 \neq r3 \neq r4 \neq r5 \neq i$ .

Accordingly, the mutation pool, composed of the Jaya mutation and DE/rand/2 mutation operations, is proposed as follows

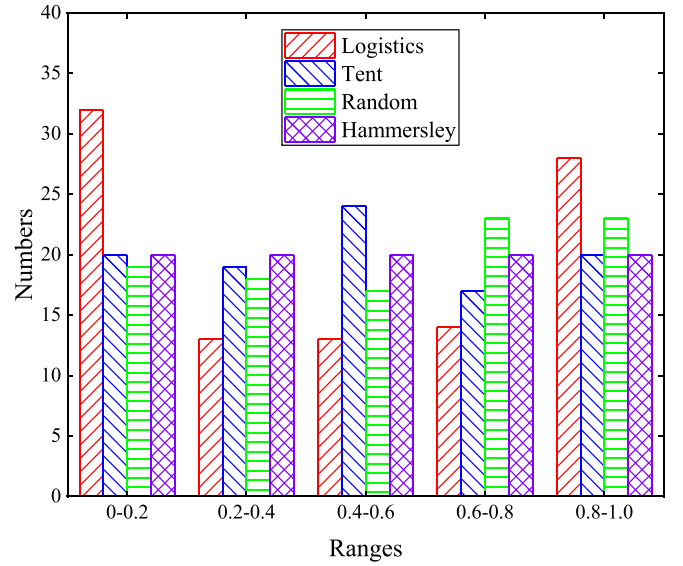


Fig. 1. Statistical results of 100 sample points generated by four methods.

$$\text{Mutation pool} = \begin{cases} \text{Jaya mutation,} & \text{if } \text{rand} < 0.5 \\ \text{DE/rand/2 mutation operation of DE,} & \text{otherwise} \end{cases} \quad (5)$$

In the proposed mutation pool, powerful exploitation capability of Jaya mutation and exploration capability of DE/rand/2 mutation are effectively integrated by implementing them in a random manner. The strengths of both methods are combined.

#### 2.1.2. Two modifications into HJDEA

##### Modification 1: Population initialization using Hammersley sequence.

Most of heuristic algorithms randomly generate the initial population within the predefined search space limits. Although this approach is simple and easy to implement, it often results in significant instability. The Hammersley sequence, a widely used low-discrepancy sequence, can generate more uniformly distributed samples in high-dimensional spaces compared to pseudo-random numbers, such as random distribution sequences and Latin hypercube sequences. Herein, population of HJDEA is initialized using Hammersley sequence. Other three methods, i.e., Logistics mapping, Tent mapping and Random sequence are compared. Fig. 1 presents the statistical results of one-dimensional distributions of 100 sample points within the  $[0, 1]$  interval generated by these initialization methods. It can be observed that the sample points generated by the Logistics mapping and Tent mapping are either too sparse or too concentrated in local regions. In contrast, the Hammersley sequence produces uniformly distributed sample points across all search ranges. Therefore, initializing the population with the Hammersley sequence ensures that the initial population uniformly covers the entire search space, thereby increasing population diversity and enhancing the optimization process.

Initial population is generated with Hammersley sequence instead of Eq. (1) within the search domain as follows

$$X_{i,j} = L_{i,j} + \psi(i,j) \times (U_{i,j} - L_{i,j}), \quad i = 1, 2, \dots, NP; \quad j = 1, 2, \dots, Dim \quad (6)$$

where  $\psi(i,j)$  stand for a sample generated by Hammersley sequence.

##### Modification 2: Refining the best solution by Lévy flight search.

As shown in Eq. (2), the search direction is related to the best-so-far solution  $X_{\text{best}}$  and it guides other individuals to move toward its position, which plays a crucial role in the whole optimization process. However, when solving complex multi-peak optimization problems, the best-so-far

**Algorithm 2** BFGS algorithm

```

Set an initial point  $\theta_0$ , convergence criteria, inverse Hessian approximation  $Y_0$ 
Evaluate the objective function of the initial point
Set  $k = 0$ 
While termination criterion is not reached do
    Calculate search direction  $d_k = -Y_k \nabla v(\theta_k)$ 
    Obtain the change of solution  $\Delta\theta_k = \beta_k d_k$ 
    Update new solution  $\theta_{k+1} = \theta_k + \Delta\theta_k$ 
    Calculate the gradient change  $\Delta y_k = \nabla v(\theta_{k+1}) - \nabla v(\theta_k)$ 
    Compute the Hessian approximation  $Y_{k+1}$  with Eq. (14)
     $k = k+1$ 
End while

```

**Fig. 2.** The pseudo-code of BFGS algorithm.

solution may be trapped into local optima, leading to premature convergence as it attracts other individuals to the same area. To address this issue, Lévy flight search is introduced by performing a random walk around the best-so-far solution to expand the search area and escape from local minima. Lévy flights are characterized by a combination of many small steps with occasional long jumps, a feature that distinguishes them from other random walks.

The second modification is refining the best-so-far solution by performing a random walk around it as follows

$$X_{best}^* = X_{best} + step \times rand(0, 1) \quad (7)$$

where  $X_{best}^*$  is the updated best-so-far solution;  $rand(0, 1)$  is the random number within  $[0, 1]$ ;  $step \times rand(0, 1)$  represents the random search

around  $X_{best}$  based on Lévy flight. step size is

$$step = 0.1 \frac{\eta}{|\nu|^{1/\lambda}} (X_r - X_{best}) \quad (8)$$

where  $X_r$  is a randomly selected individual except  $X_{best}$ ;  $\lambda$  is a parameter that controls the tail index of the distribution taken from  $[0, 2]$ ;  $\eta$  and  $\nu$  are normally distributed random variables, expressed as

$$\eta \sim N(0, \sigma_\eta^2), \quad \nu \sim N(0, \sigma_\nu^2) \quad (9)$$

where  $\sigma_\eta$  and  $\sigma_\nu$  can be calculated by

**Algorithm 1** HJDEA algorithm

```

Define the population size  $NP$ , number of unknown parameters  $Dim$ 
Set maximum iterations  $G_m$ , search space limits
Produce an initial population with Hammersley sequence by Eq. (6)
Initialize iteration number  $Iter = 1$ 
While termination criterion is not reached do
    Evaluate the objective function for each individual in the population
    Find the best solution  $X_{best}$  and the worst solution  $X_{worst}$ 
    For individual  $i = 1$  to  $NP$  do
        If  $X_i$  is the  $X_{best}$ 
            Refining the best solution by Lévy flight search using Eq. (7)
        Else
            If  $rand(0, 1) < 0.5$ 
                Update individuals with DE/rand/2 using Eq. (4)
            Else
                Update individuals with Jaya mutation using Eq. (2)
            End if
        End if
    End for
    Greedy selection strategy to keep better solution
     $Iter = Iter + 1$ 
End while
Output the identified best solution and its optimal value

```

**Fig. 3.** The pseudo-code of HJDEA.

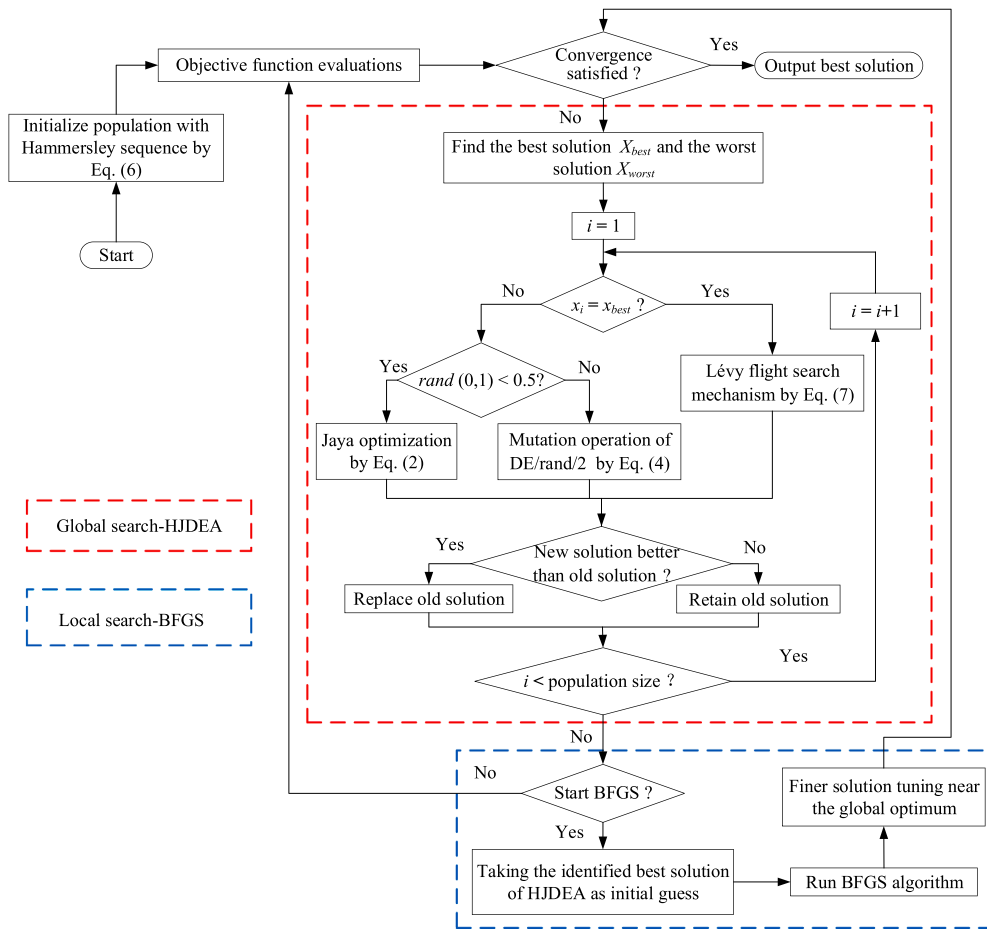


Fig. 4. The flowchart of the proposed HJDEA-BFGS algorithm.

$$\sigma_\eta = \left\{ \frac{\Gamma(1 + \lambda) \times \sin(\pi\lambda/2)}{\Gamma[(1 + \lambda)/2] \times \lambda \times 2^{(\lambda-1)/2}} \right\}^{1/\lambda}, \quad \sigma_\nu = 1 \quad (10)$$

where  $\Gamma$  represents the Gamma function.

## 2.2. HJDEA-BFGS algorithm

### 2.2.1. Introduction of BFGS algorithm

The Broyden-Fletcher-Goldfarb-Shanno (BFGS) algorithm is a popular gradient-based quasi-Newton method, widely used in solving unconstrained local optimization problems, and its iteration equation is expressed as

$$\theta_{k+1} = \theta_k + \Delta\theta_k = \theta_k + \beta_k d_k \quad (11)$$

$$d_k = -Y_k \nabla \nu(\theta_k) \quad (12)$$

where  $\theta_k$  is the solution at the  $k$ -th iteration;  $\beta_k$  means the step length;  $d_k$  represents the search direction;  $Y_k$  stands for the Hessian inverse approximation;  $\nabla \nu(\theta_k)$  is the gradient of objective function.

The gradient change  $\Delta y_k$  is calculated by

$$\Delta y_k = \nabla \nu(\theta_{k+1}) - \nabla \nu(\theta_k) \quad (13)$$

The Hessian approximation in BFGS is derived by

$$Y_{k+1} = \left( I_n - \frac{\Delta\theta_k \Delta y_k^T}{\Delta\theta_k^T \Delta y_k} \right) Y_k \left( I_n - \frac{\Delta\theta_k \Delta y_k^T}{\Delta\theta_k^T \Delta y_k} \right)^T + \frac{\Delta\theta_k \Delta\theta_k^T}{\Delta\theta_k^T \Delta y_k} \quad (14)$$

More detailed introduction about BFGS algorithm can be found in Ref. [45].

### 2.2.2. Implementation of HJDEA-BFGS algorithm

As a matter of fact, heuristic algorithms have the merits of efficient derivation-free mechanism, loose initial conditions, ease of implementation. However, they may still encounter issues such as slow convergence speed or premature convergence. To enhance the performance of HJDEA algorithm, as suggested in Ref. [29], introducing a suitable local search operator to update the best-so-far solution is one of the most effective and efficient approaches. A significant disadvantage of the BFGS method is its strong reliance on the initial guess. In multimodal objective functions, a poor initial guess may cause the search process to become stuck in a local minimum. To overcome this drawback, utilizing a high-quality solution identified by a global optimizer, such as the HJDEA algorithm, as the initial guess can be beneficial. Therefore, this study proposes a new hybrid optimization algorithm, HJDEA-BFGS, by integrating the local search operator of BFGS into the global search optimizer of HJDEA to accelerate the convergence rate to the optimal solution. The proposed HJDEA-BFGS scheme initially explores the most promising search space of unknown parameters with HJDEA, providing a good initial point that is then quickly refined by the BFGS algorithm.

The pseudo-code of BFGS is presented in Fig. 2. The detailed pseudo-code of HJDEA algorithm is presented in Fig. 3. The process of HJDEA-BFGS is illustrated in Fig. 4. After every  $N_w$  iterations of the HJDEA algorithm, the current best solution identified is further refined using the BFGS method as the initial value. Once the BFGS method reaches its maximum iterations  $M_w$ , the updated solution is compared with its initial value, and the better one is transferred back to the HJDEA algorithm as the best-so-far solution. As illustrated in Fig. 4, the flowchart of the proposed HJDEA-BFGS algorithm demonstrates a clear structure and simple operation.

### 3. Combined correlation function-based damage identification

#### 3.1. Structural damage modeling

The dynamic equation of motion for a multiple degrees of freedom (Dofs) structural system can be expressed as [8]

$$M\ddot{u}(t) + C\dot{u}(t) + Ku(t) = Bf(t) \quad (15)$$

where  $u(t)$ ,  $\dot{u}(t)$  and  $\ddot{u}(t)$  represent the structural responses of displacement, velocity and acceleration vectors, respectively;  $M$ ,  $C$ ,  $K$  mean the mass, damping and stiffness matrices;  $B$  denotes the mapping vector with the value of 1 corresponding to the force location;  $f(t)$  is the external ambient excitation. Herein, Rayleigh damping model is utilized.

A series of elemental damage vectors  $\alpha = (\alpha_1, \alpha_2, \dots, \alpha_i, \dots, \alpha_{ne})$  are introduced to describe local damage model as follows [46]

$$K_d = \sum_{i=1}^{ne} (1 - \alpha_i) K_i^e, \quad 0 \leq \alpha_i \leq 1 \quad (16)$$

where  $K_d$  and  $K_i^e$  stand for the stiffness matrix of damaged structure and the  $i$ -th elemental stiffness matrix in healthy state, respectively;  $ne$  denotes the total number of elements.  $\alpha_i = 1$  indicates the  $i$ -th element is totally damaged, and  $\alpha_i = 0$  means this element is intact. Structural parameters to be identified are  $\theta_i = 1 - \alpha_i$ ,  $i = 1, 2, \dots, ne$ .

#### 3.2. Combined correlation function of heterogeneous responses

Output-only damage detection method for civil structures under ambient excitations based on correlation functions of acceleration responses or strain responses have been developed and employed in recent years, and their detailed descriptions can be found in Refs. [36–39].

The acceleration cross-correlation function  $R_{\ddot{u}_\mu\ddot{u}_\zeta}(\tau)$  between the  $\mu$ -th and  $\zeta$ -th DOFs is written as [36]

$$R_{\ddot{u}_\mu\ddot{u}_\zeta}(\tau) = E[\ddot{x}_\mu(t)\ddot{x}_\zeta(t - \tau)] = H_{\ddot{u}_\mu\ddot{u}_\zeta}(\theta)S \quad (17)$$

where  $H_{\ddot{u}_\mu\ddot{u}_\zeta}(\theta)$  represents the convolution of the unit impulse response functions of acceleration,  $H_{\ddot{u}_\mu\ddot{u}_\zeta}(\theta) = \int_0^{+\infty} \ddot{h}_\mu(t)\ddot{h}_\zeta(t + \tau)dt$ , and it is related to unknown structural parameters;  $S$  is related to the ambient excitations.

If  $na$  accelerometers are installed on the structure, for the traditional reference point-defined method, the acceleration correlation functions  $R_{\ddot{u}_\gamma}$  with measuring point  $\gamma$  as the reference point can be expressed as

$$R_{\ddot{u}_\gamma} = [R_{\ddot{u}_{\gamma,1}}, R_{\ddot{u}_{\gamma,2}}, R_{\ddot{u}_{\gamma,3}}, \dots, R_{\ddot{u}_{\gamma,\gamma}}, \dots, R_{\ddot{u}_{\gamma,na}}] \quad (18)$$

However, in traditional reference point-defined methods, as discussed in Refs. [37–39,43], the selection of reference point for correlation functions is crucial and significantly influences the damage identification results. Poor response sensitivity to structural damage at the chosen reference point can adversely affect identification accuracy. In other words, the effectiveness of this method heavily relies on the proper selection of the reference point, presenting difficulties and challenges for practical applications. To deal with this problem, a new reference point-free method based on combined correlation function of acceleration responses is introduced as follows

$$R_{\ddot{u}} = [R_{\ddot{u}_{1,2}}, R_{\ddot{u}_{1,3}}, \dots, R_{\ddot{u}_{1,na}}, R_{\ddot{u}_{2,3}}, \dots, R_{\ddot{u}_{2,na}}, R_{\ddot{u}_{3,4}}, \dots, R_{\ddot{u}_{na-1,na}}] \quad (19)$$

Accelerometers can effectively monitor the structural health state at a global level, while damage is typically a local phenomenon. Small or minor damages may not be successfully identified using acceleration responses alone. In contrast, strain responses are more sensitive to small

damages and can capture local information if the damage is in the vicinity of strain gauges. Therefore, strain responses are used to identify structural damages. The cross-correlation function  $R_{\varepsilon_{pq}}(\tau)$  of strain responses from sensors at the locations  $p$  and  $q$  can be derived as [39]

$$R_{\varepsilon_{pq}}(\tau) = E[\varepsilon_p(t)\varepsilon_q(t - \tau)] = H_{\varepsilon_{pq}}(\theta)S \quad (20)$$

where  $H_{\varepsilon_{pq}}(\theta)$  is related to unknown structural parameters.

If  $ns$  strain gauges are installed on the structure, for the traditional reference point-defined method, the strain correlation functions  $R_{\varepsilon_\gamma}$  with measuring point  $\gamma$  as the reference point can be expressed as

$$R_{\varepsilon_\gamma} = [R_{\varepsilon_{\gamma,1}}, R_{\varepsilon_{\gamma,2}}, R_{\varepsilon_{\gamma,3}}, \dots, R_{\varepsilon_{\gamma,\gamma}}, \dots, R_{\varepsilon_{\gamma,ns}}] \quad (21)$$

The proposed reference point-free method based on the combined correlation function of strain responses is

$$R_\varepsilon = [R_{\varepsilon_{1,2}}, R_{\varepsilon_{1,3}}, \dots, R_{\varepsilon_{1,ns}}, R_{\varepsilon_{2,3}}, \dots, R_{\varepsilon_{2,ns}}, R_{\varepsilon_{3,4}}, \dots, R_{\varepsilon_{ns-1,ns}}] \quad (22)$$

In fact, various types of measurements are available for health monitoring systems installed on structures with multiple sensors. Therefore, acceleration and strain measurements could be utilized simultaneously, considering the complementary characteristics of these responses. Integrating both types of measurements enhances the effectiveness and accuracy of structural damage identification. The correlation function between acceleration response  $\ddot{u}_\mu(t)$  and strain response  $\varepsilon_p(t)$  is calculated by

$$R_{\ddot{u}_\mu\varepsilon_p}(\tau) = E[\ddot{u}_\mu(t)\varepsilon_p(t + \tau)] = H_{\ddot{u}_\mu\varepsilon_p}(\theta)S \quad (23)$$

where  $H_{\ddot{u}_\mu\varepsilon_p}(\theta)$  represents the convolution of the unit impulse response functions of acceleration and strain,  $H_{\ddot{u}_\mu\varepsilon_p}(\theta) = \int_0^{+\infty} \ddot{h}_\mu(t)\varepsilon_p(t + \tau)dt$ , and it is related to unknown structural parameters.

If the  $\gamma$ -th acceleration measurement is selected as reference point, the correlation function between acceleration response and strain response can be expressed as

$$R_{\ddot{u}_\gamma} = [R_{\ddot{u}_\gamma, \ddot{u}_1}, R_{\ddot{u}_\gamma, \ddot{u}_2}, \dots, R_{\ddot{u}_\gamma, \ddot{u}_{na}}, R_{\ddot{u}_\gamma, \varepsilon_1}, R_{\ddot{u}_\gamma, \varepsilon_2}, \dots, R_{\ddot{u}_\gamma, \varepsilon_{ns}}] \quad (24)$$

where  $na$  and  $ns$  stand for the number of accelerometers and strain gauges, respectively.

If the  $\gamma$ -th strain measurement is selected as reference point, the correlation function between acceleration response and strain response is

$$R_{\varepsilon_\gamma} = [R_{\varepsilon_\gamma, \ddot{u}_1}, R_{\varepsilon_\gamma, \ddot{u}_2}, \dots, R_{\varepsilon_\gamma, \ddot{u}_{na}}, R_{\varepsilon_\gamma, \varepsilon_1}, R_{\varepsilon_\gamma, \varepsilon_2}, \dots, R_{\varepsilon_\gamma, \varepsilon_{ns}}] \quad (25)$$

For the proposed reference point-free method, the combined correlation function of heterogeneous responses is

$$R_{\ddot{u}\varepsilon} = [R_{\ddot{u}_1, \varepsilon_2}, \dots, R_{\ddot{u}_1, \varepsilon_{na}}, \dots, R_{\ddot{u}_1, \varepsilon_{ns}}, R_{\ddot{u}_2, \varepsilon_3}, \dots, R_{\ddot{u}_2, \varepsilon_{ns}}, \dots, R_{\varepsilon_1, \varepsilon_2}, \dots, R_{\varepsilon_{ns-1}, \varepsilon_{ns}}] \quad (26)$$

Based on the proposed combined correlation function of heterogeneous responses, the objective function  $Obj$  is formulated as

$$Obj = \frac{\|R_{est} - R_{mea}\|_2}{\|R_{mea}\|_2} \quad (27)$$

where  $R_{mea}$  and  $R_{est}$  are the combined correlation function among acceleration and strain of measured and estimated data. Combined correlation function of heterogeneous responses  $R_{mea}$  can be directly computed using Eq. (26), and  $R_{est}$  is inversely calculated by  $H_{est}(H_{est}^T H_{est})^{-1} H_{est}^T R_{mea}$ .

**Table 1**  
Four classical benchmark functions for tests.

Number	Function	Name	Range	Dimension	Type
1	F1	Sphere	[-100, 100]	30	Uni-modal, Separable
2	F9	Rastrigin	[-5.12, 5.12]	30	Multi-modal, Separable
3	F10	Ackley	[-32, 32]	30	Multi-modal, Non-separable
4	F11	Griewank	[-600, 600]	30	Multi-modal, Non-separable

#### 4. Simulation and analysis

The performance of the proposed HJDEA-BFGS algorithm is initially evaluated using some representative classical benchmark functions. Subsequently, the effectiveness of the proposed output-only damage identification method for civil structures under unknown ambient excitations based on the proposed HJDEA-BFGS and combined correlation functions is verified using a series of numerical studies on the Guangzhou New TV Tower and a 39-bar three-dimensional space truss structure. All analyses are implemented in MATLAB R2020a on a personal computer. To ensure reliable identification results, 30 independent runs are conducted.

##### 4.1. Mathematical benchmark functions

In this section, four classical benchmark functions (F1, F9, F10, F11), as listed in Table 1, are utilized to validate the optimization capability of

the proposed HJDEA-BFGS. Three-dimensional plots of these four mathematical benchmark functions are shown in Fig. 5.

The proposed HJDEA-BFGS is compared with typical heuristic algorithms, namely, GA [45], DE [48], Jaya algorithm, and improved Jaya algorithm (I-Jaya) [27]. The common parameter settings for these algorithms are: population size  $NP = 100$ , maximum iterations  $G_m = 500$ , termination threshold  $= 10^{-10}$ . The adopted mutation probability and crossover probability are 0.2 and 0.8 for GA, 0.5 and 0.8 for DE. For HJDEA,  $N_w$  and  $M_w$  are set as 50 and 60, respectively. The convergence lines of four benchmark functions (F1, F9, F10, F11) based on GA, DE, Jaya, I-Jaya, and HJDEA-BFGS are presented in Fig. 6, and the total number of iterations required by each algorithm is listed in Table 2. It is evident that GA and DE encounter difficulties in solving the Rastrigin and Ackley functions because the objective function values are large beyond 500 iterations. Compared with Jaya and I-Jaya, the proposed HJDEA-BFGS achieves more superior convergence speed and much better accuracy in these four classical benchmark functions. More specifically, using the proposed hybrid optimization algorithm, only 53, 59, 66, and 85 iterations are required for F1, F9, F10, and F11, respectively, which is significantly fewer than the iterations needed by GA, DE, Jaya, I-Jaya. These results as shown in Table 2 reveal the effectiveness and efficiency of the proposed method. Therefore, HJDEA-BFGS is an attractive and promising algorithm for diverse optimization problems, including applications to damage identification of civil structures.

##### 4.2. Guangzhou New TV tower

To validate the effectiveness of the proposed method for structural

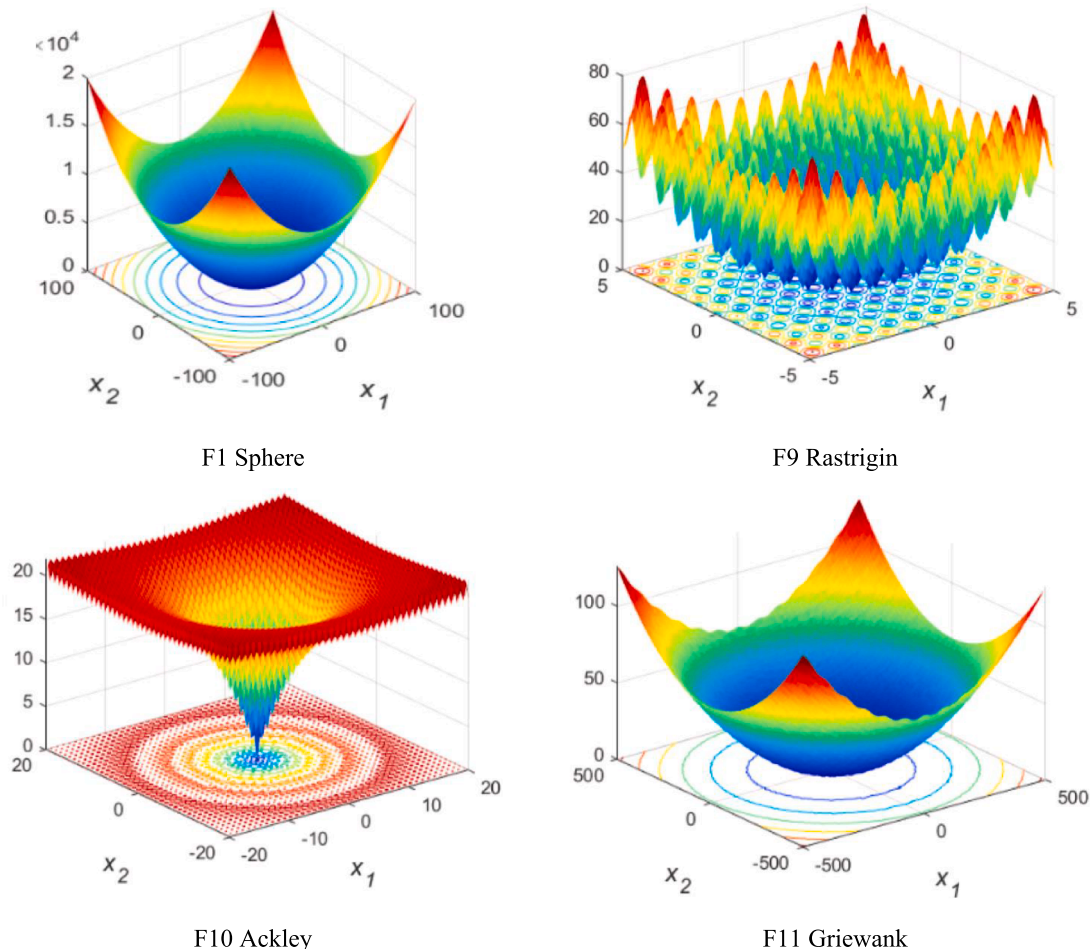


**Fig. 5.** Three-dimensional plots of four classical benchmark functions.

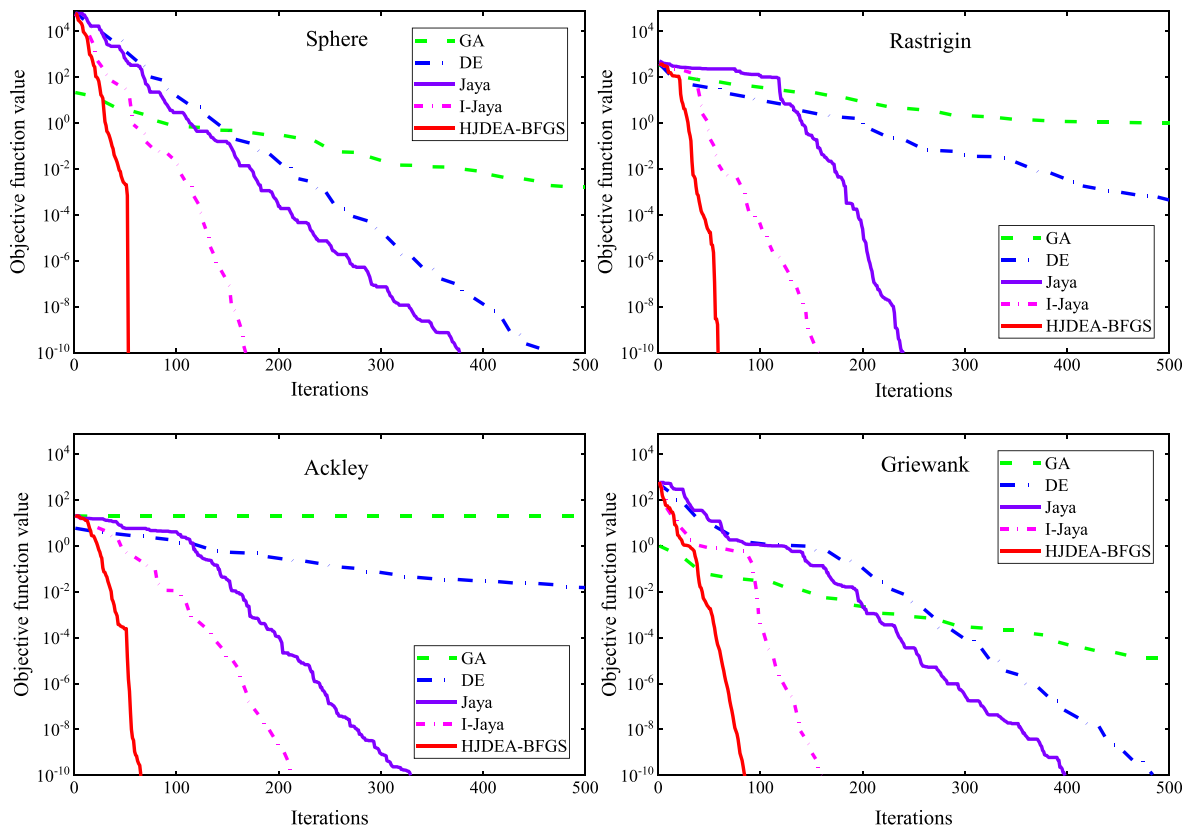


Fig. 6. The convergence process of Sphere, Rastrigin, Ackley, Griewank functions with 30 dimensions.

Table 2

The total number of iterations for GA, DE, Jaya, I-Jaya, HJDEA-BFGS.

Function	Number of iterations				
	GA	DE	Jaya	I-Jaya	HJDEA-BFGS
F1 Sphere	500	459	377	168	53
F9 Rastrigin	500	500	240	157	59
F10 Ackley	500	500	329	212	66
F11 Griewank	500	484	398	160	85

damage identification, a series of numerical studies are conducted. The Guangzhou New TV tower, as presented in Fig. 7(a), is taken as the first numerical example. As a famous landmark of Guangzhou City, the Guangzhou New TV Tower serves multiple functions, including television and radio transmission, sightseeing, dining, and entertainment. The structure has 37 floors and a total height of 610 m. To evaluate its safety during construction and operation, a structural health monitoring system with over 700 multi-type sensors was implemented. Chen et al. [49] established a full-scale 3D FEM to analyse its dynamic behaviours. This complex FEM consists of 122,476 elements, 84,370 nodes, and 505,164 DoFs. However, it is impractical to directly use such a complex model for structural damage identification. Consequently, Ni et al. [50] further simplified the FEM from the full-scale model. As shown in Fig. 7(c), the reduced-order FEM has 37 beam elements and 38 nodes. Each node has 5 Dofs, including lateral translational displacements in the x and y directions, and rotations about the x, y, and z axes. The vertical translation is not considered. As a result, the total Dofs of the reduced-order FEM are 185. The natural frequencies and modal shapes calculated from the simplified model closely match well with those of the full-scale numerical model. Therefore, the reduced-order FEM is utilized in the following studies of damage identification.

White noises with a zero mean, one standard deviations, and an amplitude of 1000 N are applied to each node to simulate ambient

excitations. Five accelerometers are installed on the 4th, 8th, 15th, 25th, and 35th floors to record the acceleration responses in the x direction. The sampling duration and sampling frequency are set to 1800 s and 200 Hz. The selection of reference points and their corresponding correlation functions are listed in Table 3. For the traditional reference point defined method, taking the acceleration of node 4 as reference point (Ref-Acc-4), the correlation functions are  $R_{4,4}$ ,  $R_{4,8}$ ,  $R_{4,15}$ ,  $R_{4,25}$ ,  $R_{4,35}$ ; Taking the measurement of node 15 as reference point (Ref-Acc-15), the correlation functions are  $R_{15,4}$ ,  $R_{15,8}$ ,  $R_{15,15}$ ,  $R_{15,25}$ ,  $R_{15,35}$ ; Taking the acceleration of node 35 as reference point (Ref-Acc-35), the correlation functions are  $R_{35,4}$ ,  $R_{35,8}$ ,  $R_{35,15}$ ,  $R_{35,25}$ ,  $R_{35,35}$ . For the proposed reference point-free method (Ref-Free), the combined correlation functions are  $R_{4,8}$ ,  $R_{4,15}$ ,  $R_{4,25}$ ,  $R_{4,35}$ ,  $R_{8,15}$ ,  $R_{8,25}$ ,  $R_{8,35}$ ,  $R_{15,25}$ ,  $R_{15,35}$ ,  $R_{25,35}$ . The first 50 data points of each correlation function are selected, resulting in a total of 500 data points used for damage identification.

In this example, there are 37 unknown parameters to be identified with only 5 acceleration responses and 37 unknown excitations. The number of sensors is less than that of external loads. To address this challenging inverse problem, the proposed HJDEA-BFGS is employed with parameters identical to those used in classical benchmark tests. Assuming there is 20 % and 20 % elemental stiffness reduction at elements 16 and 23, i.e.,  $\alpha_{16} = 0.2$ ,  $\alpha_{23} = 0.2$ , the identification results based on HJDEA-BFGS and combined correlation function (Ref-Free) with 0 %, 10 %, and 20 % noise are shown in Fig. 8. It can be found that the damaged element 16 and element 23 are successfully located and quantified. The identified mean error and maximum error are 0.25 % and 0.84 % in the noise-free case, 0.34 % and 1.29 % in the 10 % noise case, 0.26 % and 0.94 % in the 20 % noise case. Thus, the proposed combined correlation function demonstrates good robustness to noise and can accurately identify the elemental stiffness damages under multiple unknown ambient excitations. For comparison purposes, GA [45], GBABC [51], Jaya, HJDEA are also used to detect damages of Guangzhou New TV tower. As shown in Table 4, GA, GBABC and basic

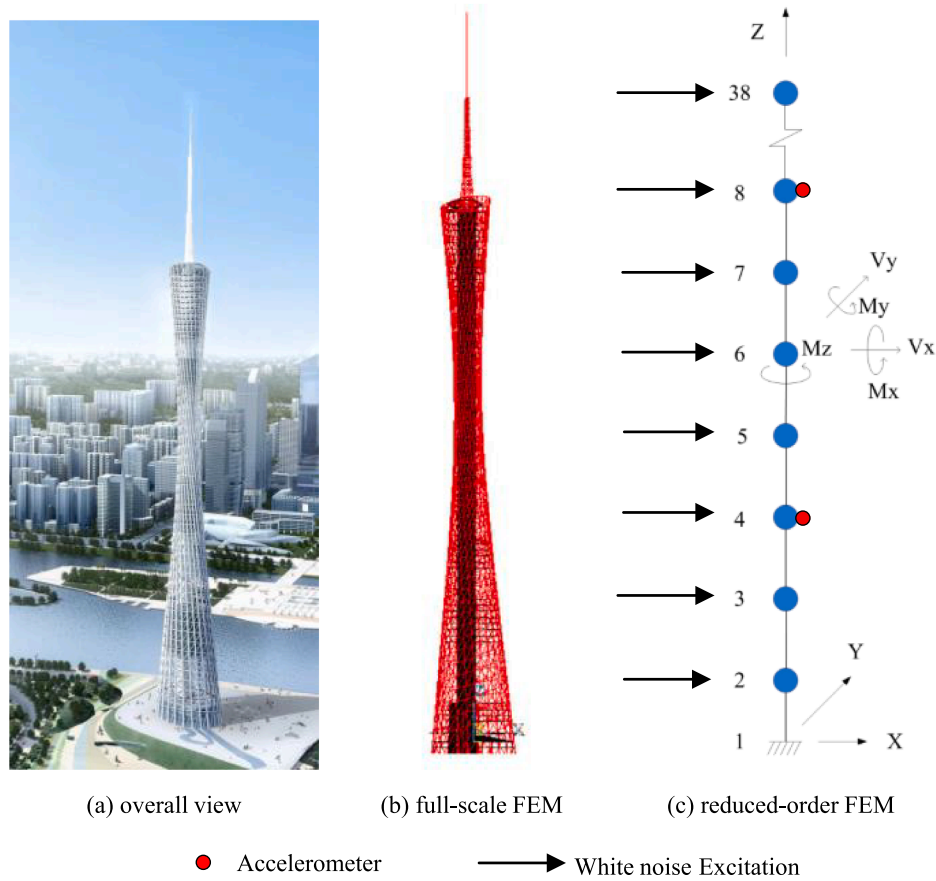


Fig. 7. Guangzhou New TV Tower and its simplified finite element model.

Table 3

Selection of reference point and their correlation functions for the Guangzhou New TV Tower.

Methods	Name	Location of accelerations	Correlation functions
Acceleration as reference point	Ref-Acc-4	4th (Ref), 8th, 15th, 25th, and 35th floors	$R_{4,4}, R_{4,8}, R_{4,15}, R_{4,25}, R_{4,35}$
	Ref-Acc-15	4th, 8th, 15th (Ref), 25th, and 35th floors	$R_{15,4}, R_{15,8}, R_{15,15}, R_{15,25}, R_{15,35}$
	Ref-Acc-35	4th, 8th, 15th, 25th, and 35th (Ref) floors	$R_{35,4}, R_{35,8}, R_{35,15}, R_{35,25}, R_{35,35}$
	Combined correlation function	Ref-Free and 35th floors	$R_{4,8}, R_{4,15}, R_{4,25}, R_{4,35}, R_{8,15}, R_{8,25}, R_{8,35}, R_{15,25}, R_{15,35}, R_{25,35}$

Jaya algorithm could not provide accurate results, with maximum errors exceeding 10 % in the 20 % noise case. In contrast, the performance of HJDEA is acceptable with less than 5 % error alarm. The proposed HJDEA-BFGS yields the best results with, with a maximum error of only 1.29 %, due to the effective integration of the powerful global search optimizer HJDEA and the efficient local search operator BFGS.

Furthermore, the identified results using the traditional reference point defined method, i.e., Ref-Acc-4, Ref-Acc-15, Ref-Acc-35, are listed in Table 4. Obviously, Ref-Acc-4 provides the worst identification results with mean error and maximum error exceeding 4.9 % and 14.3 % respectively when contaminated with 20 % noise. Ref-Acc-15 can achieve better results than Ref-Acc-4, but the maximum errors are 6.81 %, 7.11 %, and 8.06 % for the 0 %, 10 %, and 20 % noise cases, respectively, which exceed the acceptable range for false alarms to some extent. Ref-Acc-35 obtains the most satisfactory results among Ref-Acc-4, Ref-Acc-15, and Ref-Acc-35, but still performs worse than the proposed Ref-Free

method. This study demonstrates the selection of reference points significantly affects the detected results. Improper selection of reference point may result in unaccepted false identifications, whereas the Ref-Free method can avoid incorrect damage identification results caused by an improper selection of reference point.

In summary, the favorable performance of the HJDEA-BFGS algorithm in solving optimization-based damage identification for the Guangzhou New TV Tower implies that the proposed method is both effective and robust. It successfully identifies structural damages even with 20 % noise-contaminated output-only responses by optimizing the combined correlation function-based objective function. This demonstrates the potential for structural health monitoring under various noise conditions.

#### 4.3. Three-dimensional space truss structure

The accuracy and effectiveness of the proposed method are further verified by a numerical example of three-dimensional space truss structure. As shown in Fig. 9, the truss has a length of 1.0 m, a width of 0.5 m, and a total height of 3 m. It consists of 16 nodes and 39 truss elements. Each bar has a circular cross-section with an outer diameter of 20 mm and a thickness of 2 mm. Each node has three Dofs, and the bottom supports at nodes 1, 2, 3, and 4 are constrained. Hence, the space truss has a total of 36 Dofs. The material used for the three-dimensional truss is steel. The Young's modulus and mass density are  $2.10 \times 10^{11} \text{N/m}^2$  and  $7850 \text{kg/m}^3$ , respectively.

A Rayleigh damping model is used with damping coefficients calculated from the first two modes. In order to simulate the dynamic behavior of the three-dimensional space truss structure under ambient excitations, multiple white noise excitations are applied in the x direction at nodes 5, 8, 9, 12, 13, and 16, and in the y direction at nodes 7, 8,

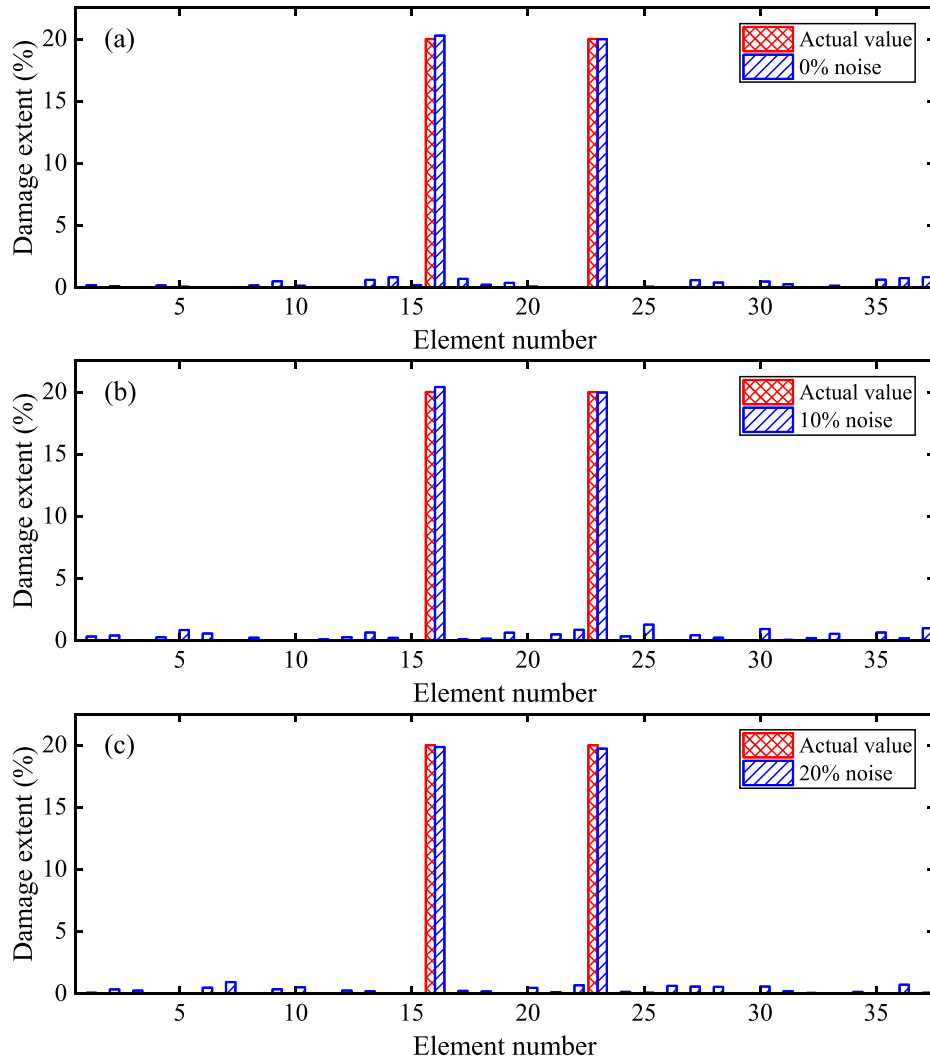


Fig. 8. Damage identification results of the Guangzhou New TV Tower using HJDEA-BFGS and Ref-free method: (a) 0% noise; (b) 10% noise; (c) 20% noise.

Table 4  
Statistical results of GA, GBABC, Jaya, HJDEA, HJDEA-BFGS algorithms.

Methods	Algorithms	Noise free		10 % noise		20 % noise	
		Mean	Max	Mean	Max	Mean	Max
Ref-Free	GA	5.67	28.66	5.34	32.08	5.82	30.13
	GBABC	2.94	9.92	3.06	8.48	3.65	14.03
	Jaya	1.83	8.19	1.65	8.51	1.76	10.36
	HJDEA	0.77	3.43	1.11	4.12	1.02	4.47
	HJDEA-BFGS	0.25	0.84	0.34	1.29	0.26	0.94
Ref-Acc-4	HJDEA-BFGS	5.06	14.72	5.19	16.58	4.97	14.34
Ref-Acc-15	HJDEA-BFGS	2.20	6.81	2.63	7.11	2.23	8.06
Ref-Acc-35	HJDEA-BFGS	1.26	4.50	1.09	5.44	1.17	5.06

11, 12, 15, and 16. Four accelerometers measure the acceleration responses in the x direction at nodes 6 and 9, and in the y direction at nodes 8 and 15, i.e.,  $\ddot{u}_{6(x)}$ ,  $\ddot{u}_{9(x)}$ ,  $\ddot{u}_{8(y)}$ ,  $\ddot{u}_{15(y)}$ . Additionally, strain responses from elements 2, 17, 26, and 34 are collected, i.e.,  $\epsilon_2$ ,  $\epsilon_{17}$ ,  $\epsilon_{26}$ ,  $\epsilon_{34}$ . Thus, there are four acceleration responses and four strain responses in total. The sampling duration is 1800 s and the sampling frequency is 1000 Hz. Assuming there are 30 %, 20 %, and 10 % stiffness reductions in the 13th, 21th, and 30th elements, respectively, which

means  $\alpha_{13} = 0.3$ ,  $\alpha_{21} = 0.2$ ,  $\alpha_{30} = 0.1$ .

#### 4.3.1. Comparison of reference point free and defined method

For heterogeneous responses including acceleration and strain measurements, damage identification results vary when either acceleration response or strain response is used as the reference point in the reference point-defined method. Moreover, the specific acceleration or strain data selected as the reference point also impacts the final damage detection results. To address these issues, a reference point-free method based on the combined correlation function is proposed in Section 2.2. This section compares the performance of the proposed reference point-free method with the reference point-defined methods in terms of damage identification accuracy and robustness. As listed in Table 5, three methods are considered: acceleration as reference point (Ref-Acc), strain as reference point (Ref-Strain), and the combined correlation function (Ref-Free). For the Ref-Acc method, the acceleration response at node 9 in the x direction is selected as reference point, expressed as Ref-Acc-9(x). For the Ref-Strain method, the strain response at element 17 is selected as reference point, expressed as Ref-Strain-17. For the Ref-Free method, the combined correlation functions are  $R_{6(x),9(x)}$ ,  $R_{6(x),8(y)}$ ,  $R_{6(x),15(y)}$ ,  $R_{6(x),2}$ ,  $R_{6(x),17}$ ,  $R_{6(x),26}$ ,  $R_{6(x),34}$ ,  $R_{9(x),8(y)}$ ,  $R_{9(x),15(y)}$ ,  $R_{9(x),2}$ ,  $R_{9(x),17}$ ,  $R_{9(x),26}$ ,  $R_{9(x),34}$ ,  $R_{8(y),15(y)}$ ,  $R_{8(y),2}$ ,  $R_{8(y),17}$ ,  $R_{8(y),26}$ ,  $R_{8(y),34}$ ,  $R_{15(y),2}$ ,  $R_{15(y),17}$ ,  $R_{15(y),26}$ ,  $R_{15(y),34}$ ,  $R_{2,17}$ ,  $R_{2,26}$ ,  $R_{2,34}$ ,  $R_{17,26}$ ,  $R_{17,34}$ ,  $R_{26,34}$ . This method involves 6 acceleration-acceleration correlation functions, 6 strain-strain correlation functions, and 16 acceleration-strain

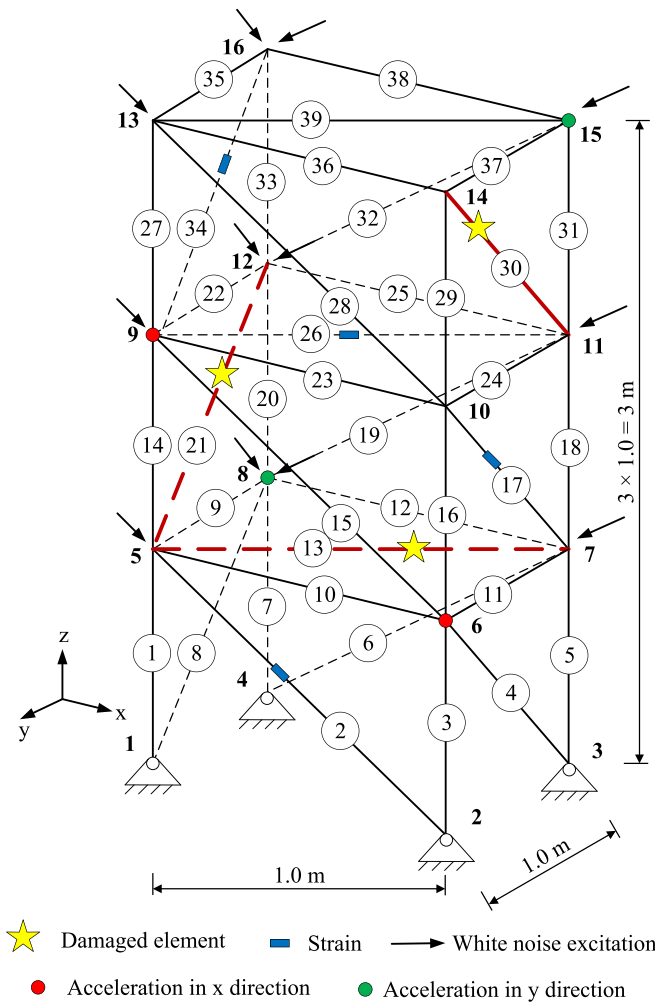


Fig. 9. Three-dimensional space truss structure.

**Table 5**  
Selection of reference point and their correlation functions for the truss structure.

Methods	Location of accelerations	Location of strains	Correlation functions
Ref-Acc-9(x)	6(x), 9(x)(Ref), 8(y), 15(y)	2, 17, 26, 34	$R_{9(x),6(x)}, R_{9(x),9(x)}, R_{9(x),8(y)}, R_{9(x),15(y)}, R_{9(x),2}, R_{9(x),17}, R_{9(x),26}, R_{9(x),34}$
Ref-Strain-17	6(x), 9(x), 8(y), 15(y)	2, 17 (Ref), 26, 34	$R_{17,6(x)}, R_{17,9(x)}, R_{17,8(y)}, R_{17,15(y)}, R_{17,2}, R_{17,17}, R_{17,26}, R_{17,34}$
Combined correlation function Ref-Free	6(x), 9(x), 8(y), 15(y)	2, 17, 26, 34	$R_{6(x),9(x)}, R_{6(x),8(y)}, R_{6(x),15(y)}, R_{6(x),2}, R_{6(x),17}, R_{6(x),26}, R_{6(x),34}, R_{9(x),8(y)}, R_{9(x),15(y)}, R_{9(x),2}, R_{9(x),17}, R_{9(x),26}, R_{9(x),34}, R_{8(y),15(y)}, R_{8(y),2}, R_{8(y),17}, R_{8(y),26}, R_{8(y),34}, R_{15(y),2}, R_{15(y),17}, R_{15(y),26}, R_{15(y),34}, R_{2,17}, R_{2,26}, R_{2,34}, R_{17,26}, R_{17,34}, R_{26,34}$

correlation functions. The first 50 data points of these 28 correlation functions are used to evaluate the objective function. The proposed hybrid optimization algorithm HJDEA-BFGS is utilized to identify damages in the 39-bar three-dimensional space truss structure subjected to multiple unknown ambient excitations. Identification results for Ref-Acc-9(x), Ref-Strain-17 and Ref-Free using HJDEA-BFGS are presented in Fig. 10 and Table 6.

As shown in Fig. 10, the identified damage extents of elements 13, 21 and 30 are 30.95 %, 19.10 % and 2.12 % when taking the acceleration response of node 9(x) as the reference point (Ref-Acc-9(x)). There are large identification errors, nearly 8 %, at the 8th and 17th elements. When using the strain response from element 17 as the reference point (Ref-Strain-17), it is not feasible to accurately locate the damaged elements or quantify the degree of damage. In contrast, using the proposed combined correlation functions of heterogeneous responses (Ref-Free), the position and extent of the damaged elements can be successfully located and accurately identified with a small mean error of 0.55 % only and a maximum error 3.05 %. Compared with the Ref-Acc-9(x) and Ref-Strain-17, the proposed Ref-Free method can not only avoid incorrect damage identification results caused by the improper selection of a reference point, but also further improve the accuracy of damage detection since more acceleration-acceleration correlation functions, acceleration-strain correlation functions, and strain-strain correlation functions are involved in objective function evaluation. Thus, the superiority of the proposed Ref-Free method is reasonably validated by the results.

#### 4.3.2. Comparisons with other heuristic algorithms

To further verify the performance of the proposed HJDEA-BFGS, comparisons with GA, GBABC, Jaya, and HJDEA are conducted. Three noise levels are considered to study the adverse effect of noise on the damage identification results. The identified errors with these five intelligent optimization algorithms are shown in Table 6. The maximum errors for the GA, GBABC, Jaya, and HJDEA algorithms are 28.66 %, 9.92 %, 8.19 %, and 5.78 % in the noise-free case, respectively, which are significantly larger than the acceptable range. In contrast, the maximum identification error of HJDEA-BFGS is less than 1.5 % even under 10 % and 20 % noise conditions, demonstrating the robustness of the combined correlation function to noise. The proposed HJDEA-BFGS algorithm exhibits stronger optimization capabilities since the local optimizer BFGS can improve solution accuracy by refining the current best solution. Therefore, HJDEA-BFGS achieves better accuracy compared with GA, GBABC, Jaya, and HJDEA, as presented in Fig. 11 and Table 6. The simulated damages at the 13th, 21th, and 30th elements are accurately detected with only minor errors observed. These results demonstrate that the proposed structural damage identification method, based on HJDEA-BFGS and combined correlation function of heterogeneous responses, can accurately identify structural damage location and degree under unknown ambient excitations.

## 5. Discussions

Discussions on various conditions, such as different noise levels, sampling frequencies, sampling durations and number of data points, will inevitably require considerable computing resources, especially for large and complex structures, which is not conducive to efficient analysis and conclusion. Hence, to save computational time, a relatively simple 10-Dofs structure is used to further analyze the effects of noise level, sampling frequency, sampling duration, and the number of data points on damage identification results with the proposed approach. Fig. 12 presents the setup of the 10-Dofs shear-type structure [47]. The stiffness and mass parameters are listed in Table 7. Random excitations with a mean value of zero, unit standard deviation, and amplitude of 200 N are horizontally applied to each floor. Three accelerometers are installed on the 1st, 5th, and 9th floors to collect horizontal acceleration responses. The sampling duration is 1800 s and the sampling frequency is 100 Hz. The combined correlation function of acceleration response  $R = [R_{1,5}, R_{1,9}, R_{5,9}]$  is calculated. The first 50 data points of  $R_{1,5}, R_{1,9}, R_{5,9}$ , 150 data points in total, are selected for damage identification. It is assumed that elements 3 and 8 have stiffness damage of 30 % and 20 %, respectively, i.e.,  $\alpha_3 = 0.3, \alpha_8 = 0.2$ . The parameter settings of HJDEA used are: population size  $NP = 60$ , maximum iterations  $G_m = 100$ ,  $N_w = 30$ ;  $M_w = 20$ .

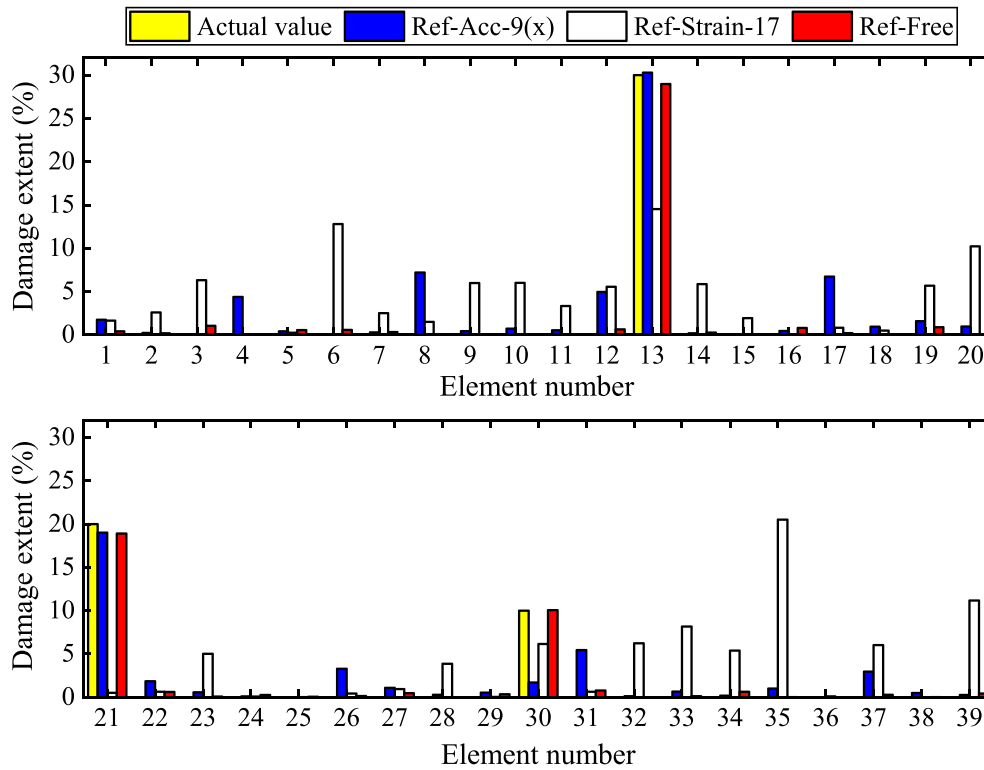


Fig. 10. Identification results for Ref-Acc-9(x), Ref-Strain-17 and Ref-Free using HJDEA-BFGS without noise.

Table 6 Identification errors with GA, GBABC, Jaya, HJDEA, and HJDEA-BFGS (%).

Methods	Algorithm	Noise free		10 % noise		20 % noise	
		Mean	Max	Mean	Max	Mean	Max
Ref-Acc-9 (x)	HJDEA-BFGS	1.54	8.30	1.63	8.46	1.70	7.61
Ref-Strain-17	HJDEA-BFGS	4.66	20.51	5.02	24.82	4.76	26.17
Ref-Free	GA	5.67	28.66	5.34	32.08	5.82	30.26
	GBABC	2.94	9.92	3.06	8.48	3.33	14.21
	Jaya	1.83	8.19	1.65	8.51	1.71	10.58
	HJDEA	1.06	5.78	0.93	5.24	1.19	5.60
	HJDEA-BFGS	0.32	1.09	0.28	1.27	0.34	1.10

5.1. Effect of noise level

To account for the adverse effects of measurement noise, Gaussian white noise is added to the numerically obtained acceleration data [52]. Four noise levels, 0 %, 10 %, 20 %, and 30 %, are considered. The damage identification results using HJDEA-BFGS are shown in Fig. 13. The average errors at noise levels of 0 %, 10 %, 20 %, and 30 % are 0.28 %, 0.33 %, 0.47 %, 0.39 %, respectively, with maximum errors of 1.04 %, 1.25 %, 1.36 %, 1.60 %. Notably, the maximum identification error does not exceed 2 % even with 30 % noise, indicating that the combined correlation function proposed in this paper exhibits good robustness to noise. Fig. 14(a) shows the acceleration time history of the first five seconds of the fifth floor with and without measurement noise, demonstrating that the acceleration response is susceptible to measurement noise. Fig. 14(b) shows the time history of the cross-correlation function  $R_{5,9}$  under 0 % and 20 % noise levels. It is observed that the curves almost overlap. The relative error (RE) and Pearson correlation coefficient (PCC) are  $RE = 1.47 %$  and  $PCC = 0.9989$ . These results indicate that the method based on the combined correlation function is insensitive to noise.

5.2. Effect of sampling frequency

The first 10 natural frequencies of the 10-Dofs frame structure are 0.76 Hz, 1.98 Hz, 3.29 Hz, 4.47 Hz, 5.63 Hz, 6.59 Hz, 7.43 Hz, 7.98 Hz, 8.75 Hz, and 9.25 Hz. Six different sampling frequencies, i.e., 5 Hz, 10 Hz, 20 Hz, 50 Hz, 100 Hz, and 200 Hz, are used to study their effects on the identification results. Fig. 15 shows the identification errors associated with these sampling frequencies. It can be observed that as the sampling frequency increases, the average identification error gradually decreases. When the sampling frequencies are 5 Hz and 10 Hz, the maximum identification error exceeds 6 %, while smaller identification errors are obtained when the sampling frequency is larger than 20 Hz. These results imply that it is difficult to obtain the response information of the high-order modes at relatively low sampling frequency, which is not conducive to the accurate identification of local damage. Therefore, the sampling frequency should be reasonably selected according to the natural frequencies of the target structure.

5.3. Effect of sampling duration

Six different sampling durations, 5 min, 10 min, 20 min, 30 min, 40 min, and 60 min, are considered to study their effects on the identification results. Fig. 16 shows the identification errors associated with different sampling times. It can be observed that the identification errors gradually decrease as the sampling time increases. When the sampling time does not exceed 20 min, the maximum identification error exceeds 3 %. However, after the sampling time exceeds 30 min, the identification errors only slightly change. As shown in Table 8, the computational time also increases significantly with longer sampling duration. Thus, blindly increasing the sampling duration may not further improve identification accuracy but consume more computational resources. Therefore, to save computational costs, it is important to choose an appropriate sampling time within an acceptable error range.

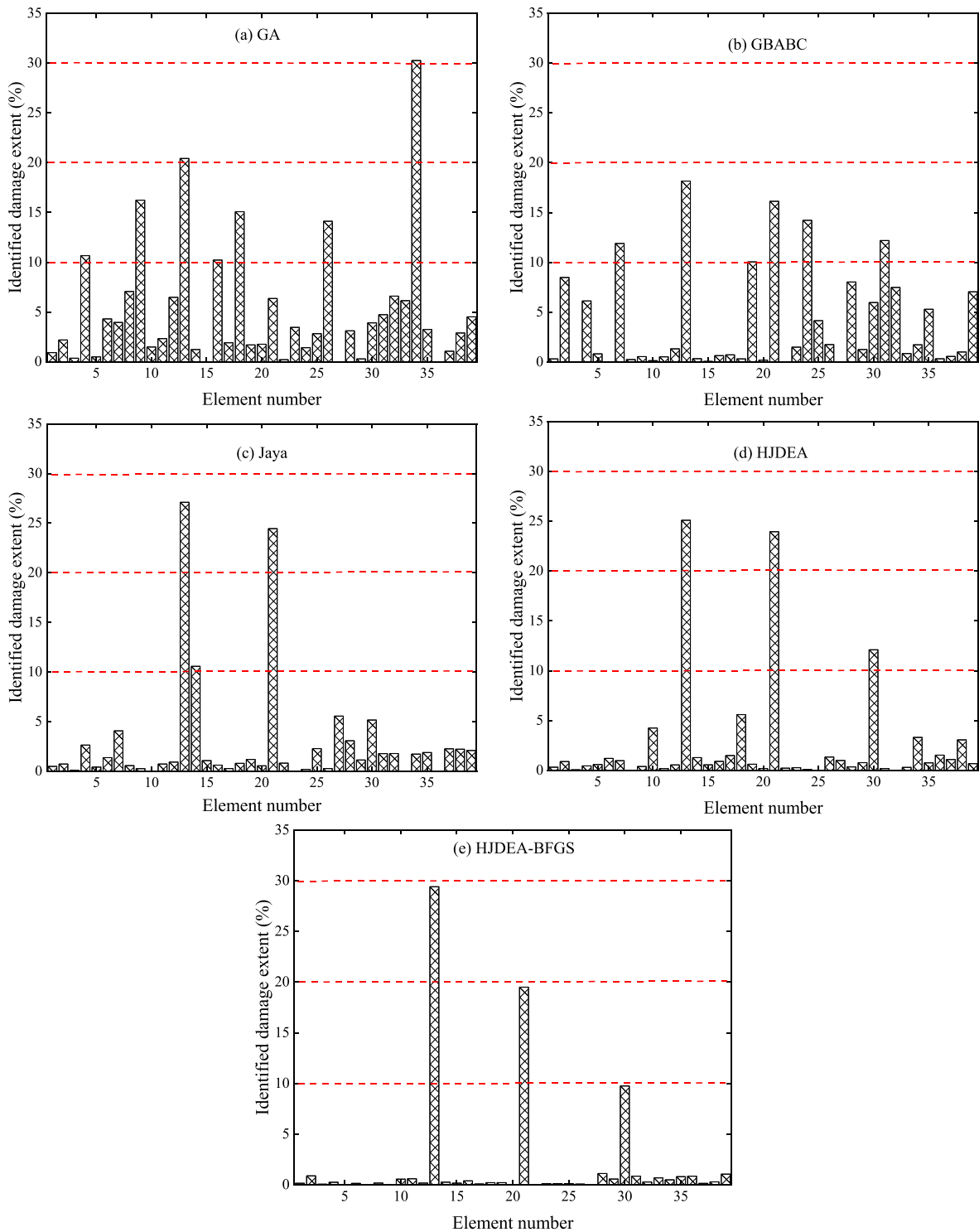


Fig. 11. Identified results using five different heuristic algorithms and Ref-free method under 20% noise: (a) GA; (b) GBABC; (c) Jaya; (d) HJDEA; (e) HJDEA-BFGS.

5.4. Effect of number of data points

It is necessary to determine the number of data points using the combined correlation function  $R = [R_{1,5}, R_{1,9}, R_{5,9}]$ . Six different numbers of data points, i.e., 50, 100, 150, 200, 250, and 300, are considered to study their impact on computational efficiency and identification accuracy. By the results in Fig. 17 and Table 9, the maximum identification errors are 1.52 % and 4.37 % for data points of 100 and 300, with computational times of 288.6 s and 859.5 s. It can be observed that using more data points may not improve the accuracy of

the results, instead, it consumes more computational resources. To further investigate this phenomenon, the relative errors between the measured combined correlation function  $R_{mea}$  and the estimated combined correlation function  $R_{est}$  are analyzed. As shown in Table 9, the relative errors between the measured and estimated values accumulate as the number of data points increases, negatively impacting the accuracy of the identification results due to noise accumulation with more data points. Therefore, considering both computational efficiency and identification accuracy, it is necessary to choose reasonable number of data points.

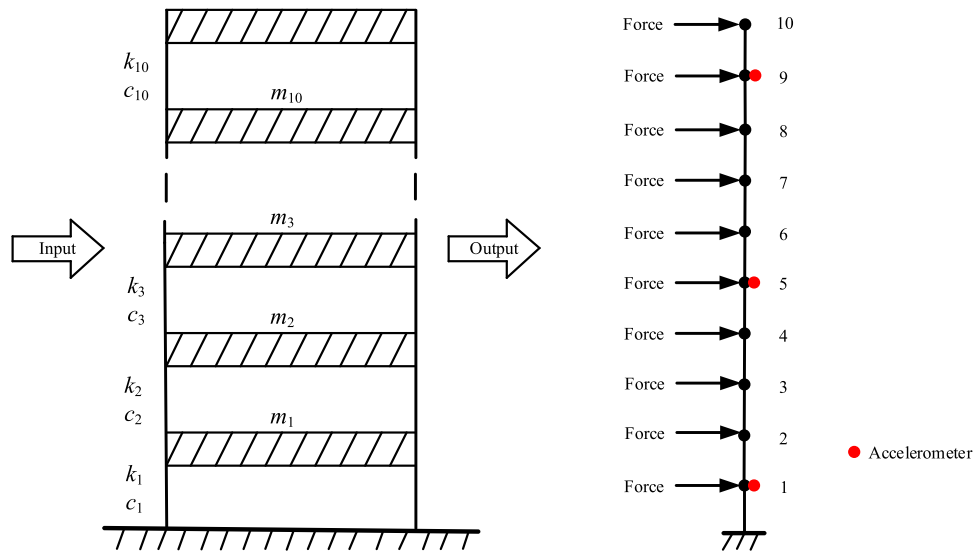


Fig. 12. Numerical model of 10-Dofs frame structure.

**Table 7**  
Structural parameters of 10-Dofs structure.

Structural parameters	Floors	Values
Stiffness	1–4	5000 (kN/m)
	5–8	4000 (kN/m)
	9–10	3000 (kN/m)
Mass	1–5	6000 (kg)
	6–10	4200 (kg)

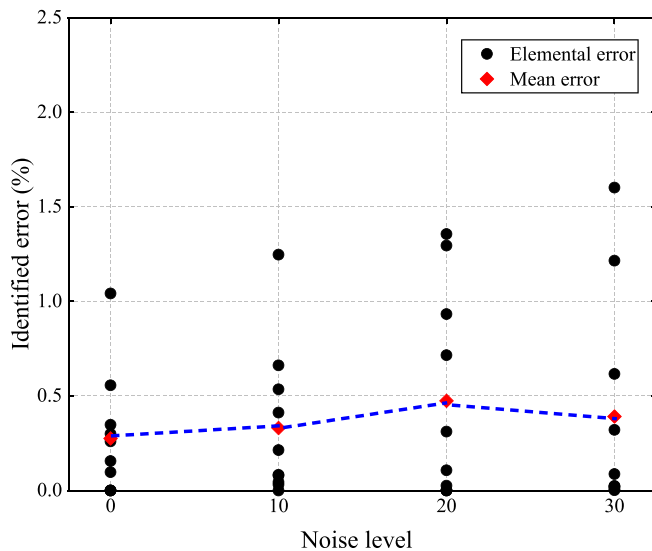


Fig. 13. Damage identification results under different noise.

## 6. Conclusions

This paper proposes a novel approach for damage detection of civil structures subjected to ambient excitations using the HJDEA-BFGS and a combined correlation function of heterogeneous responses to address

the challenges including the selection of reference point in traditional correlation function-based methods and the limitations of single-method optimization strategies. In this approach, the hybrid optimization algorithm HJDEA-BFGS is developed by integrating the local search optimizer of BFGS into the global search optimizer of HJDEA. A new objective function is established based on the combined correlation function among hybrid acceleration and strain measurements. Some high-dimension classical benchmark functions are used to evaluate the performance of the proposed HJDEA-BFGS, comparing its results with those of existing heuristic algorithms. Numerical examples, including the Guangzhou New TV Tower and a 39-bar three-dimensional space truss structure subjected to ambient excitations, validate the applicability and effectiveness of the proposed method. Furthermore, the effects of noise levels, sampling times, sampling frequencies, and the number of data points are discussed to facilitate the implementation of the proposed method. Some conclusions can be drawn from these studies:

- (1) The proposed output-only damage identification method based on HJDEA-BFGS and the combined correlation function of heterogeneous responses can achieve less than 0.4 % mean error for varying damage scenarios and maintains robustness under noise levels up to 20 %, demonstrating its reliability for real-world applications.
- (2) The maximum identification error of HJDEA-BFGS is less than 1.5 % even under 10 % and 20 % noise conditions, demonstrating the robustness of the combined correlation function to noise. The hybrid strategy of HJDEA-BFGS achieves more accurate and robust damage identification results than GA, GBABC, Jaya, and HJDEA.
- (3) The selection of a reference point significantly impacts the final identification results. Improper selection of a reference point can lead to false identifications. The proposed combined correlation function, as a reference point-free method, outperforms traditional reference point-defined methods and exhibits strong robustness to noise.
- (4) Selecting an appropriate sampling frequency that corresponds to the natural frequencies of the target structure is crucial for accurately capturing high-order mode responses. Excessively

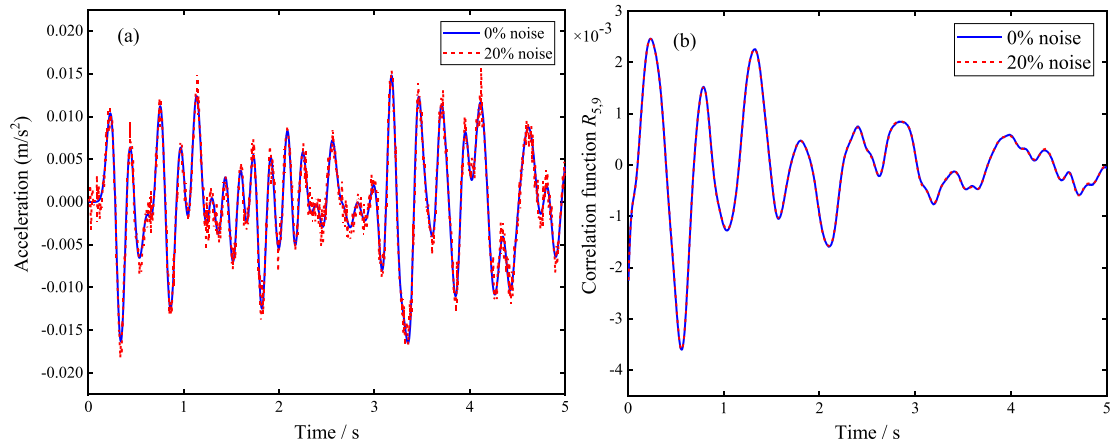


Fig. 14. Comparison of time histories: (a) acceleration with 0% and 20% noise; (b) correlation function with 0% and 20% noise.

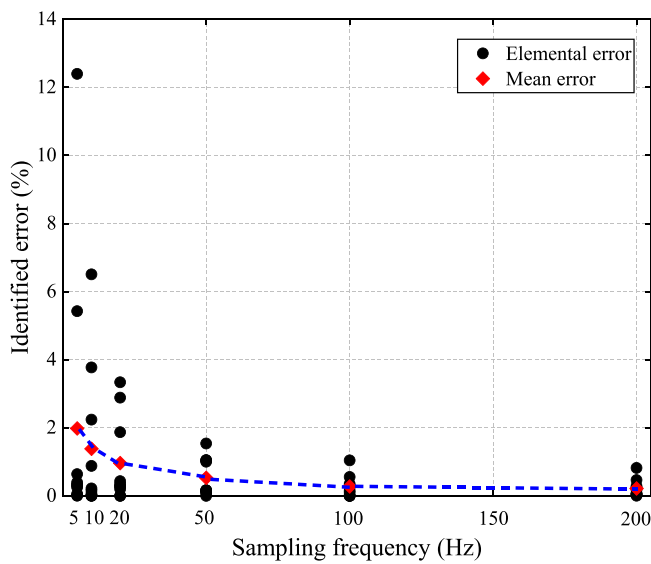


Fig. 15. Identified errors with different sampling frequencies.

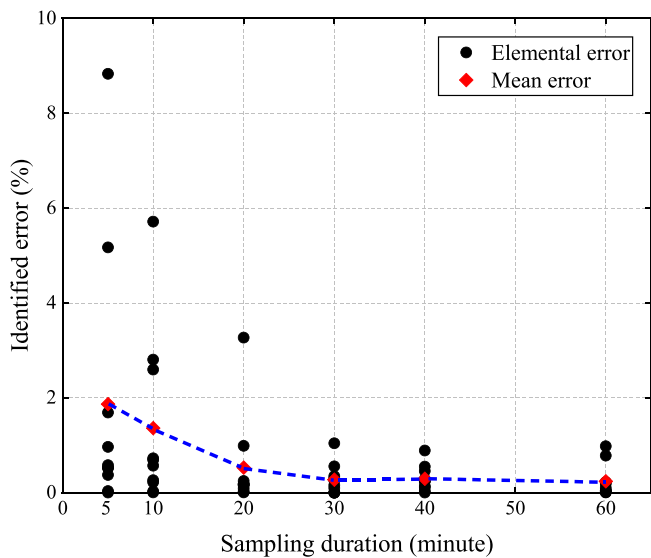


Fig. 16. Identified errors with different sampling durations.

Table 8

Identified results with different sampling times (%).

Sampling duration (min)	Error		Standard deviation	Calculation time (s)
	Mean value	Maximum error		
5	1.87	8.83	2.02	173.8
10	1.36	5.72	1.45	183.6
20	0.53	3.27	0.86	201.9
30	0.28	1.04	0.42	217.3
40	0.29	0.89	0.34	246.1
60	0.24	0.98	0.31	297.2

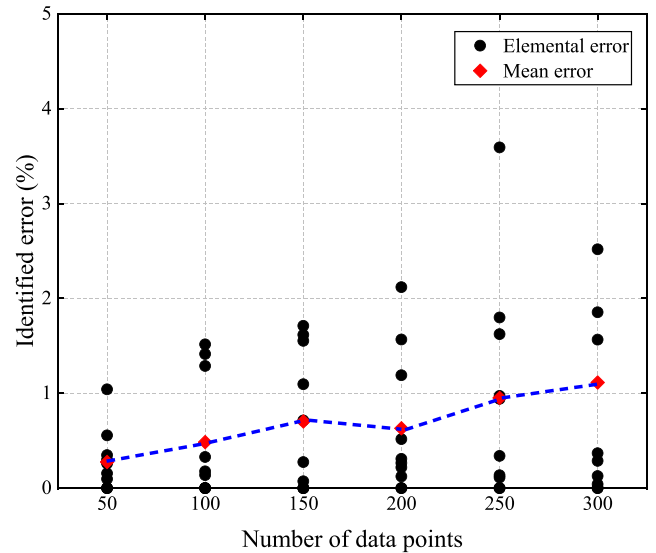


Fig. 17. Identified errors with different numbers of data points.

increasing the sampling duration does not necessarily improve identification accuracy but increases computational costs.

Some aspects are not considered in the present paper, such as modeling errors, temperature variation, boundary stiffness alteration, and optimal sensor placement. The effectiveness of the proposed method is validated using numerical examples, which might not capture the full complexity of real-world structural conditions. Scaled model experiments in the laboratory and field measurement data will be used to validate the method in future studies. Exploring the integration of additional heterogeneous data types, such as non-contact vision-based

**Table 9**  
Identified results with different numbers of data points (%).

Number of data points	Errors		Standard deviation	Time (s)	Data points	Relative error between measured and calculated correlation function		
	Mean	Max				$R_{1,5}$	$R_{1,9}$	$R_{5,9}$
50	0.28	1.04	0.55	196.7	1–50	0.83	0.68	4.32
100	0.49	1.52	0.41	288.6	51–100	2.91	1.58	1.07
150	0.70	1.71	0.63	465.9	101–150	3.33	4.05	4.53
200	0.63	2.12	0.58	578.1	151–200	2.57	2.77	2.42
250	0.95	3.59	0.95	739.2	201–250	3.28	3.62	4.59
300	1.11	4.37	1.13	859.5	251–300	4.63	3.46	5.34

displacement measurement for enhanced damage detection robustness. Additionally, the method will be adapted for application to other structural types, such as plates and trusses, to further validate its versatility and robustness.

### CRedit authorship contribution statement

**Guangcai Zhang:** Writing – original draft, Validation, Software, Methodology, Investigation, Conceptualization. **Chunfeng Wan:** Writing – review & editing, Supervision, Formal analysis. **Zhiyuan Yang:** Visualization, Software, Resources. **Liyu Xie:** Writing – review & editing, Supervision. **Songtao Xue:** Writing – review & editing, Supervision, Funding acquisition.

### Declaration of competing interest

The authors declare that they have no known competing financial interests or personal relationships that could have appeared to influence the work reported in this paper.

### Acknowledgments

This research is supported by: the National Key R&D Program of China (2021YFE0112200), the Japan Society for Promotion of Science (Kakenhi No. 18 K04438), the Tohoku Institute of Technology research Grant and the Postgraduate Research&Practice Innovation Program of Jiangsu Province (KYCX23\_0273). These financial supports are sincerely appreciated. Besides, the author would like to thank the anonymous reviewers for their detailed and fruitful remarks.

### Data availability

Data will be made available on request.

### References

- [1] W. Fan, P. Qiao, Vibration-based damage identification methods: a review and comparative study[J], *Struct. Health Monit.* 10 (1) (2011) 83–111.
- [2] M.S. Dizaji, M. Alipour, D.K. Harris, Subsurface damage detection and structural health monitoring using digital image correlation and topology optimization[J], *Eng. Struct.* 230 (2021) 111712.
- [3] G. Zhang, J. Hou, C. Wan, et al., Non-contact vision-based response reconstruction and reinforcement learning guided evolutionary algorithm for substructural condition assessment[J], *Mech. Syst. Sig. Process.* 224 (2025) 112017.
- [4] O. Avci, O. Abdeljaber, S. Kiranyaz, et al., A review of vibration-based damage detection in civil structures: From traditional methods to Machine Learning and Deep Learning applications[J], *Mech. Syst. Sig. Process.* 147 (2021) 107077.
- [5] I. Zacharakis, D. Giagopoulos, Vibration-based damage detection using finite element modeling and the metaheuristic particle swarm optimization algorithm[J], *Sensors* 22 (14) (2022) 5079.
- [6] B. Bhowmik, T. Tripura, B. Hazra, et al., Robust linear and nonlinear structural damage detection using recursive canonical correlation analysis[J], *Mech. Syst. Sig. Process.* 136 (2020) 106499.
- [7] G. Gui, H. Pan, Z. Lin, et al., Data-driven support vector machine with optimization techniques for structural health monitoring and damage detection[J], *KSCSE J. Civ. Eng.* 21 (2017) 523–534.
- [8] M.J. Perry, C.G. Koh, Output-only structural identification in time domain: numerical and experimental studies[J], *Earthq. Eng. Struct. Dyn.* 37 (4) (2008) 517–533.
- [9] Y. Li, S. Wang, J. Tapia, et al., An iterative total least squares-based estimation method for structural damage identification of 3D frame structures[J], *Struct. Control Health Monit.* 27 (4) (2020) e2499.
- [10] J. Li, H. Hao, Substructure damage identification based on wavelet-domain response reconstruction[J], *Struct. Health Monit.* 13 (4) (2014) 389–405.
- [11] D. Ginsberg, C.P. Fritzen, O. Loffeld, Sparsity-constrained extended Kalman filter concept for damage localization and identification in mechanical structures[J], *Smart Struct. Syst.* 21 (6) (2018) 741–749.
- [12] F. Cadini, C. Sbarufatti, M. Corbetta, et al., Particle filtering-based adaptive training of neural networks for real-time structural damage diagnosis and prognosis, *Struct. Control Health Monit.* 26 (12) (2019) e2451.
- [13] C. Song, E. Shang, X. Huang, et al., Monitoring the cohesive damage of the adhesive layer in CFRP double-lapped bonding joint based on non-uniform strain profile reconstruction using dynamic particle swarm optimization algorithm[J], *Measurement* 123 (2018) 235–245.
- [14] T.T. Truong, D. Dinh-Cong, J. Lee, et al., An effective deep feedforward neural networks (DFNN) method for damage identification of truss structures using noisy incomplete modal data[J], *Journal of Building Engineering* 30 (2020) 101244.
- [15] M.H. Sulaiman, Z. Mustafa, Using the evolutionary mating algorithm for optimizing the user comfort and energy consumption in smart building[J], *Journal of Building Engineering* 76 (2023) 107139.
- [16] S.A. Ansari, A. Zafar, A fusion of dolphin swarm optimization and improved sine cosine algorithm for automatic detection and classification of objects from surveillance videos[J], *Measurement* 192 (2022) 110921.
- [17] V. Meruane, W. Heylen, Damage detection with parallel genetic algorithms and operational modes[J], *Struct. Health Monit.* 9 (6) (2010) 481–496.
- [18] Z. Ding, J. Li, H. Hao, et al., Structural damage identification with uncertain modelling error and measurement noise by clustering based tree seeds algorithm [J], *Eng. Struct.* 185 (2019) 301–314.
- [19] P. Ghannadi, S.S. Kourehli, M. Noori, et al., Efficiency of grey wolf optimization algorithm for damage detection of skeletal structures via expanded mode shapes [J], *Adv. Struct. Eng.* 23 (13) (2020) 2850–2865.
- [20] Y. Li, L. Zhao, Y. Wang, et al., Improved sand cat swarm optimization algorithm for enhancing coverage of wireless sensor networks[J], *Measurement* 233 (2024) 114649.
- [21] S. Hassani, U. Dackermann, M. Mousavi, et al., Enhanced damage detection for noisy input signals using improved reptile search algorithm and data analytics techniques[J], *Comput. Struct.* 296 (2024) 107293.
- [22] C. Yang, Interval strategy-based regularization approach for force reconstruction with multi-source uncertainties[J], *Comput. Methods Appl. Mech. Eng.* 419 (2024) 116679.
- [23] M.H. Daneshvar, M. Saffarian, H. Jahangir, et al., Damage identification of structural systems by modal strain energy and an optimization-based iterative regularization method[J], *Eng. Comput.* 39 (3) (2023) 2067–2087.
- [24] C. Yang, A novel uncertainty-oriented regularization method for load identification [J], *Mech. Syst. Sig. Process.* 158 (2021) 107774.
- [25] R. Rao, Jaya: A simple and new optimization algorithm for solving constrained and unconstrained optimization problems[J], *Int. J. Ind. Eng. Comput.* 7 (1) (2016) 19–34.
- [26] G. Zhang, C. Wan, L. Xie, et al., Structural damage identification with output-only measurements using modified Jaya algorithm and Tikhonov regularization method [J], *Smart Struct. Syst.* 31 (3) (2023) 229.
- [27] G. Zhang, C. Wan, S. Xue, et al., A global-local hybrid strategy with adaptive space reduction search method for structural health monitoring[J], *App. Math. Model.* 121 (2023) 231–251.
- [28] K. Belhadj, A. Helali, N.B. Guedria, et al., Damage assessment in plate structures using an enhanced Jaya algorithm[J], *Eng. Optim.* (2024) 1–29.
- [29] Z. Ding, R. Hou, Y. Xia, Structural damage identification considering uncertainties based on a Jaya algorithm with a local pattern search strategy and L0. 5 sparse regularization[J], *Eng. Struct.* 261 (2022) 114312.
- [30] E.H. Houssein, B.E. Helmy, H. Rezk, et al., An enhanced Archimedes optimization algorithm based on Local escaping operator and Orthogonal learning for PEM fuel cell parameter identification[J], *Eng. Appl. Artif. Intell.* 103 (2021) 104309.
- [31] V. Kelner, F. Capitanescu, O. Léonard, et al., A hybrid optimization technique coupling an evolutionary and a local search algorithm[J], *J. Comput. Appl. Math.* 215 (2) (2008) 448–456.
- [32] H. Sun, H. Waisman, R. Betti, Nondestructive identification of multiple flaws using XFEM and a topologically adapting artificial bee colony algorithm[J], *Int. J. Numer. Meth. Eng.* 95 (10) (2013) 871–900.

- [33] J.Y. Wu, Y. Huang, V.P. Nguyen, On the BFGS monolithic algorithm for the unified phase field damage theory[J], *Comput. Methods Appl. Mech. Eng.* 360 (2020) 112704.
- [34] H. Cui, X. Xu, W. Peng, et al., A damage detection method based on strain modes for structures under ambient excitation[J], *Measurement* 125 (2018) 438–446.
- [35] M. Zhang, Y. Li, X. Peng, et al., Damage Assessment Using the Auto-Correlation-Function-Based Damage Index[J], *International Journal of Acoustics & Vibration* 28 (3) (2023).
- [36] G. Zhang, C. Wan, X. Xiong, et al., Output-only structural damage identification using hybrid Jaya and differential evolution algorithm with reference-free correlation functions[J], *Measurement* 199 (2022) 111591.
- [37] P. Ni, Y. Xia, S.S. Law, et al., Structural damage detection using auto/cross-correlation functions under multiple unknown excitations[J], *Int. J. Struct. Stab. Dyn.* 14 (05) (2014) 1440006.
- [38] X. Wang, G. Zhang, X. Wang, et al., Output-only structural parameter identification with evolutionary algorithms and correlation functions[J], *Smart Mater. Struct.* 29 (3) (2020) 035018.
- [39] G. Zhang, J. Hou, K. Feng, et al., Structural damage identification with output-only strain measurements and swarm intelligence algorithms: a comparative study[J], *Meas. Sci. Technol.* 35 (5) (2024) 056125.
- [40] M. Li, W.X. Ren, T.L. Huang, et al., Experimental investigations on the cross-correlation function amplitude vector of the dynamic strain under varying environmental temperature for structural damage detection[J], *Journal of Low Frequency Noise, Vibration and Active Control* 39 (3) (2020) 631–649.
- [41] N.T. Davis, M. Sanayei, Foundation identification using dynamic strain and acceleration measurements[J], *Eng. Struct.* 208 (2020) 109811.
- [42] H. Hasni, P. Jiao, A.H. Alavi, et al., Structural health monitoring of steel frames using a network of self-powered strain and acceleration sensors: A numerical study [J], *Autom. Constr.* 85 (2018) 344–357.
- [43] X. Wang, F. Chen, H. Zhou, et al., Structural damage detection based on cross-correlation function with data fusion of various dynamic measurements[J], *J. Sound Vib.* 541 (2022) 117373.
- [44] M.Y. Zhang, Z.C. Yang, L. Wang, et al., Damage locating for composite beam structure by cross correlation analysis without reference node[J], *Engineering Mechanics* 28 (11) (2011) 166–169.
- [45] Z. Zhang, C.G. Koh, W.H. Duan, Uniformly sampled genetic algorithm with gradient search for structural identification—Part II: Local search[J], *Comput. Struct.* 88 (19–20) (2010) 1149–1161.
- [46] C.S.N. Pathirage, J. Li, L. Li, et al., Structural damage identification based on autoencoder neural networks and deep learning[J], *Eng. Struct.* 172 (2018) 13–28.
- [47] M.J. Perry, C.G. Koh, Y.S. Choo, Modified genetic algorithm strategy for structural identification[J], *Comput. Struct.* 84 (8–9) (2006) 529–540.
- [48] L.T. Stutz, R.A. Tenenbaum, R.A.P. Correa, The Differential Evolution method applied to continuum damage identification via flexibility matrix[J], *J. Sound Vib.* 345 (2015) 86–102.
- [49] W.H. Chen, Z.R. Lu, W. Lin, et al., Theoretical and experimental modal analysis of the Guangzhou New TV Tower[J], *Eng. Struct.* 33 (12) (2011) 3628–3646.
- [50] Y.Q. Ni, Y. Xia, W. Lin, et al., SHM benchmark for high-rise structures: a reduced-order finite element model and field measurement data[J], *Smart Struct. Syst.* 10 (4–5) (2012) 411–426.
- [51] X. Zhou, Z. Wu, H. Wang, et al., Gaussian bare-bones artificial bee colony algorithm[J], *Soft. Comput.* 20 (2016) 907–924.
- [52] A. Malekjafarian, F. Golpayegani, C. Moloney, et al., A machine learning approach to bridge-damage detection using responses measured on a passing vehicle[J], *Sensors* 19 (18) (2019) 4035.